Article

Cell Reports

Role of Selenof as a Gatekeeper of Secreted Disulfide-Rich Glycoproteins

Graphical Abstract

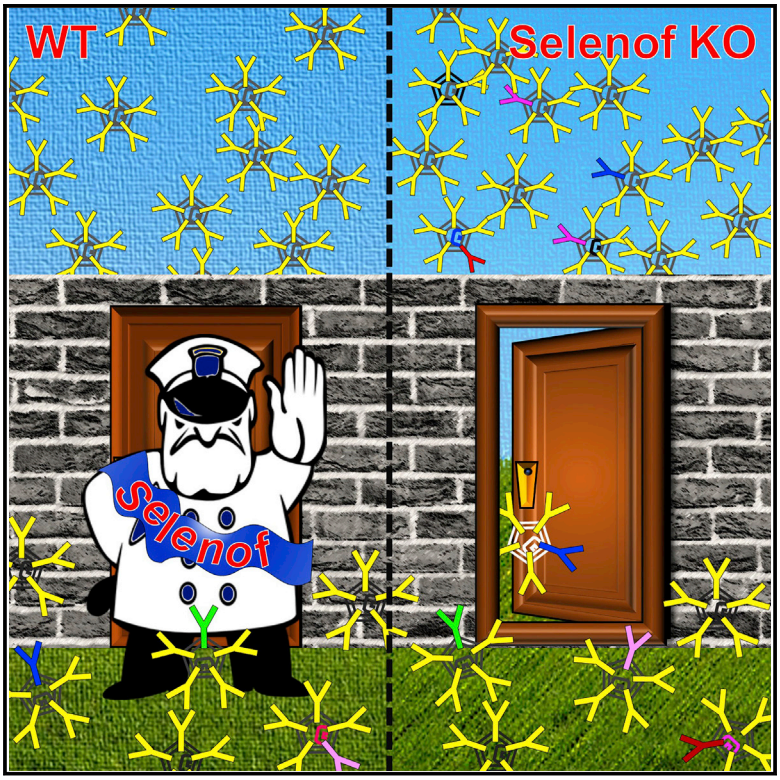

Authors

Sun Hee Yim, Robert A. Everley, Frank A. Schildberg, ..., Arlene H. Sharpe, Dolph L. Hatfield, Vadim N. Gladyshev

Correspondence

vgladyshev@rics.bwh.harvard.edu

In Brief

Yim et al. report that Selenof (15-kDa selenoprotein; Sep15) functions as a gatekeeper of immunoglobulins and, likely, other client proteins en route from the ER to the Golgi apparatus, thereby preventing secretion of dysfunctional proteins and supporting redox quality control.

Highlights

- Selenof deficiency elevates levels of plasma immunoglobulins
- IgM secretion is higher in Selenof knockout B cells
- Elevated IgM does not increase antimicrobial capacity or systemic IgM activity
- Selenof facilitates antigen presentation via ER-to-Golgi transport

Yim et al., 2018, Cell Reports *23*, 1387–1398
May 1, 2018
https://doi.org/10.1016/j.celrep.2018.04.009

CellPress

Cell Reports
Article

Role of Selenof as a Gatekeeper of Secreted Disulfide-Rich Glycoproteins

Sun Hee Yim,[1] Robert A. Everley,[2] Frank A. Schildberg,[3] Sang-Goo Lee,[1] Andrea Orsi,[4] Zachary R. Barbati,[3] Kutay Karatepe,[5] Dmitry E. Fomenko,[6] Petra A. Tsuji,[7] Hongbo R. Luo,[5] Steven P. Gygi,[2] Roberto Sitia,[4] Arlene H. Sharpe,[3] Dolph L. Hatfield,[8] and Vadim N. Gladyshev[1,9,*]

[1]Division of Genetics, Department of Medicine, Brigham and Women's Hospital, Harvard Medical School, Boston, MA 02115, USA
[2]Department of Cell Biology, Harvard Medical School, Boston, MA 02115, USA
[3]Department of Microbiology and Immunobiology and Evergrande Center for Immunologic Diseases, Harvard Medical School, Boston, MA 02115, USA
[4]Division of Genetics and Cell Biology, IRCCS Ospedale San Raffaele and Università Vita-Salute San Raffaele, Milano, Italy
[5]Department of Pathology and Lab Medicine, Children's Hospital Boston, Harvard Medical School, Boston, MA 02115, USA
[6]Redox Biology Center and Computational Science Initiative, University of Nebraska–Lincoln, Lincoln, NE 68588, USA
[7]Department of Biological Sciences, Towson University, Towson, MD 21252, USA
[8]Molecular Biology of Selenium Section, Mouse Cancer Genetics Program, National Cancer Institute, NIH, 9000 Rockville Pike, Bethesda, MD 20892, USA
[9]Lead Contact
*Correspondence: vgladyshev@rics.bwh.harvard.edu
https://doi.org/10.1016/j.celrep.2018.04.009

SUMMARY

Selenof (15-kDa selenoprotein; Sep15) is an endoplasmic reticulum (ER)-resident thioredoxin-like oxidoreductase that occurs in a complex with UDP-glucose:glycoprotein glucosyltransferase. We found that Selenof deficiency in mice leads to elevated levels of non-functional circulating plasma immunoglobulins and increased secretion of IgM during *in vitro* splenic B cell differentiation. However, Selenof knockout animals show neither enhanced bacterial killing capacity nor antigen-induced systemic IgM activity, suggesting that excess immunoglobulins are not functional. In addition, ER-to-Golgi transport of a target glycoprotein was delayed in Selenof knockout embryonic fibroblasts, and proteomic analyses revealed that Selenof deficiency is primarily associated with antigen presentation and ER-to-Golgi transport. Together, the data suggest that Selenof functions as a gatekeeper of immunoglobulins and, likely, other client proteins that exit the ER, thereby supporting redox quality control of these proteins.

INTRODUCTION

Selenium is an essential trace element due to its occurrence in proteins in the form of selenocysteine (Sec, U). Sec is known as the 21st amino acid encoded by a UGA codon; it is inserted co-translationally into nascent polypeptides with the help of the Sec insertion sequence (SECIS) element (Berry et al., 1991). There are 25 selenoprotein genes in humans and 24 in mice and most other mammals (Kryukov et al., 2003). Functionally characterized selenoproteins serve thiol oxidoreductase functions with Sec located in enzyme active sites and are directly involved in catalysis. More than half of the mammalian selenoproteins are characterized by a thioredoxin fold, with Sec occupying the position of the catalytic redox cysteine (Cys) in thioredoxin (Labunskyy et al., 2014; Reeves and Hoffmann, 2009).

Selenof (Selenoprotein F; 15-kDa selenoprotein; Sep15) (Gladyshev et al., 1998) is one of the 25 selenoproteins encoded in the human genome. It consists of an endoplasmic reticulum (ER)-targeting signal peptide, an N-terminal Cys-rich domain, and a C-terminal thioredoxin-like domain (Labunskyy et al., 2009). While it is an ER-resident selenoprotein, Selenof lacks the ER retention signal. However, it binds UDP-glucose:glycoprotein glucosyltransferase (UGGT), an ER-resident glycoprotein folding sensor, through its Cys-rich domain. Thus, binding to UDP-glucose supports Selenof retention in the ER (Korotkov et al., 2001; Labunskyy et al., 2009). UGGT recognizes incompletely folded glycoproteins and targets them to the calnexin-calreticulin-ERp57 system by reglucosylation, thereby allowing another cycle of maturation (Caramelo and Parodi, 2008; Hammond et al., 1994; Trombetta and Helenius, 2000). This function prevents an ER-to-Golgi exit of folding intermediates, misfolded glycoproteins, and immature multimeric complexes, ensuring that only properly folded glycoproteins are targeted to other cellular compartments, reach the cell surface, and are secreted (Anelli and Sitia, 2008; Cabral et al., 2001; Sousa et al., 1992; Zuber et al., 2001). Prevention of secretion of dysfunctional proteins is complex and specific to particular protein classes, but it is not well defined (Frand et al., 2000; Spang, 2013).

The tight binding between Selenof and UGGT implies that Selenof may also be involved in ER quality control, but this possibility has been difficult to test. It was found that UGGT occurs in both Selenof-bound and Selenof-free forms, whereas the entire pool of Selenof binds UGGT (Korotkov et al., 2001). The enzyme activities of both of UGGT1 and UGGT2 are enhanced by the formation of a complex with Selenof (Ito et al., 2015; Takeda et al., 2014). Selenof exhibits a redox potential suggestive of a reductase or isomerase function, rather than an

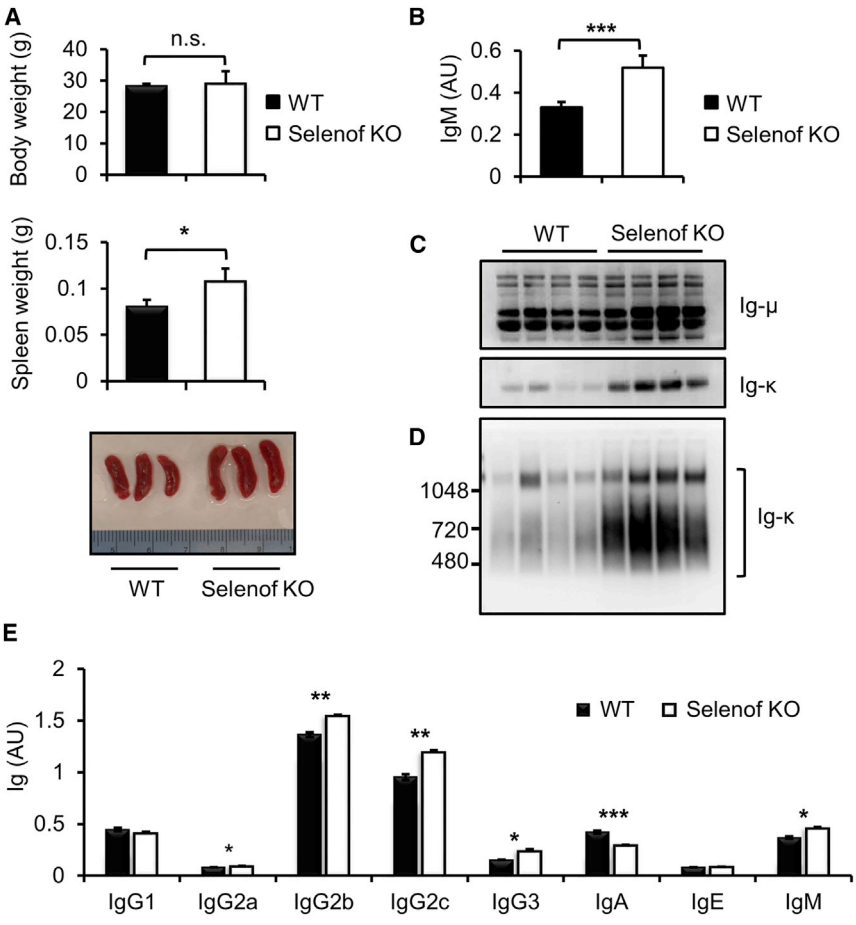

Figure 1. Selenof Deficiency Leads to Elevated Immunoglobulin Levels

(A) Body and spleen weights of WT and Selenof KO mice (n = 4 per group). Spleen weights are different between WT and Selenof KO mice ($p = 0.02$). 13-week old WT and Selenof KO littermates were used.

(B) IgM analyses in WT and Selenof KO mouse sera by ELISA. The sera were diluted to 1:12,000, and anti-IgM antibody was used as a capture antibody. 13-week-old littermates (n = 4 per group) were used.

(C and D) Aliquots of sera from WT and Selenof KO mice were resolved under reducing SDS-PAGE (C) or 4–16% non-reducing NativePAGE (D), and blots were analyzed with anti-Ig-μ or anti-Ig-κ antibodies. 10 μg serum protein per lane was loaded.

(E) Immunoglobulins were quantified in WT and Selenof KO sera by ELISA. Blood was withdrawn from the submandibular vein of 12-week-old male littermates (n = 8 per group). Sera were diluted to 1:50,000, and anti-Ig (H+L) was used as a capture antibody. Two-tailed probability values of a Student's t test are as follows: IgG2a, $p = 0.03$; IgG2b, $p = 0.006$; IgG2c, $p = 0.002$; IgG3, $p = 0.02$; IgA, $p = 0.0004$; and IgM, $p = 0.02$.

Data are expressed as mean ± SD. *$p < 0.05$; **$p < 0.01$; ***$p < 0.001$; n.s., not significant.

oxidase of Cys residues (Ferguson et al., 2006; Labunskyy et al., 2009). Thus, it is an attractive possibility that Selenof supports redox quality control for a subset of UGGT client proteins. In this regard, some secreted glycoproteins, such as immunoglobulins (Igs) that are exceptionally disulfide rich, are potential clients for the UGGT/Selenof sensor. These proteins may be exemplified by IgM, which is the major antibody produced upon primary immune response. It is expressed in B cells and circulates in the blood of all vertebrate species (Cenci and Sitia, 2007; Ehrenstein and Notley, 2010). IgM is often used to identify acute exposure to an immunogen or pathogen (Leijh et al., 1979). It triggers the opsonization of antigens (e.g., infectious microorganisms) and causes ingested microorganisms to be promptly destroyed by phagocytes. Glycosylation of IgM is vital to its B cell surface presentation and secretion (Arnold et al., 2007; Sitia et al., 1984). Secretory IgM consists of 21 subunits, has a total 51 N-glycans, and contains 98 intra- and inter-chain disulfide bonds (Hendershot and Sitia, 2005). Like glycosylation, disulfide formation in newly synthesized proteins destined for secretion is an error-prone process (Dejgaard et al., 2004; Hatahet and Ruddock, 2009). Protein disulfide isomerase and several other ER-resident thiol oxidoreductases have been extensively studied, but much of this research focused on the actual process of disulfide bond formation and isomerization. On the other hand, redox quality control of secreted glycoproteins has not been thoroughly addressed.

In the present study, by examining the consequences of Selenof deficiency in mice and primary plasma B cell differentiation models (Bertolotti et al., 2010), we observed elevated secretion of Igs, without evidence of enhanced immune function or phenotypes associated with the secretory cells. Mouse embryonic fibroblasts (MEFs) treated with chemicals that perturb ER-to-Golgi transport reduced Selenof protein expression, while tunicamycin treatment, which induces unfolded protein response, elevated Selenof protein levels. In a fluorescence-microscopy-based assay for ER-to-Golgi transport of the vesicular stomatitis virus (VSV) G protein, Selenof knockout (KO) MEFs exhibited a significantly delayed transport function. Proteomic analyses showed depletion of "antigen presentation" and enrichment of "ER-to-Golgi anterograde transport" in Selenof KO MEFs. Together with other analyses, the data suggested that Selenof serves a function as a gatekeeper for Igs and likely other disulfide-rich glycoproteins, thereby providing redox quality control of secreted glycoproteins.

RESULTS

Systemic Selenof Deficiency in Mice Leads to Elevated Ig Levels without Altering Immune Functions

Selenof KO mice were fertile, grew and developed normally, and had no obvious pathologies. However, while wild-type (WT) and Selenof KO mice had similar body weights, the latter animals were characterized by mild splenomegaly (n = 6 per group, $p = 0.02$) (Figure 1A). By further examining littermate WT and

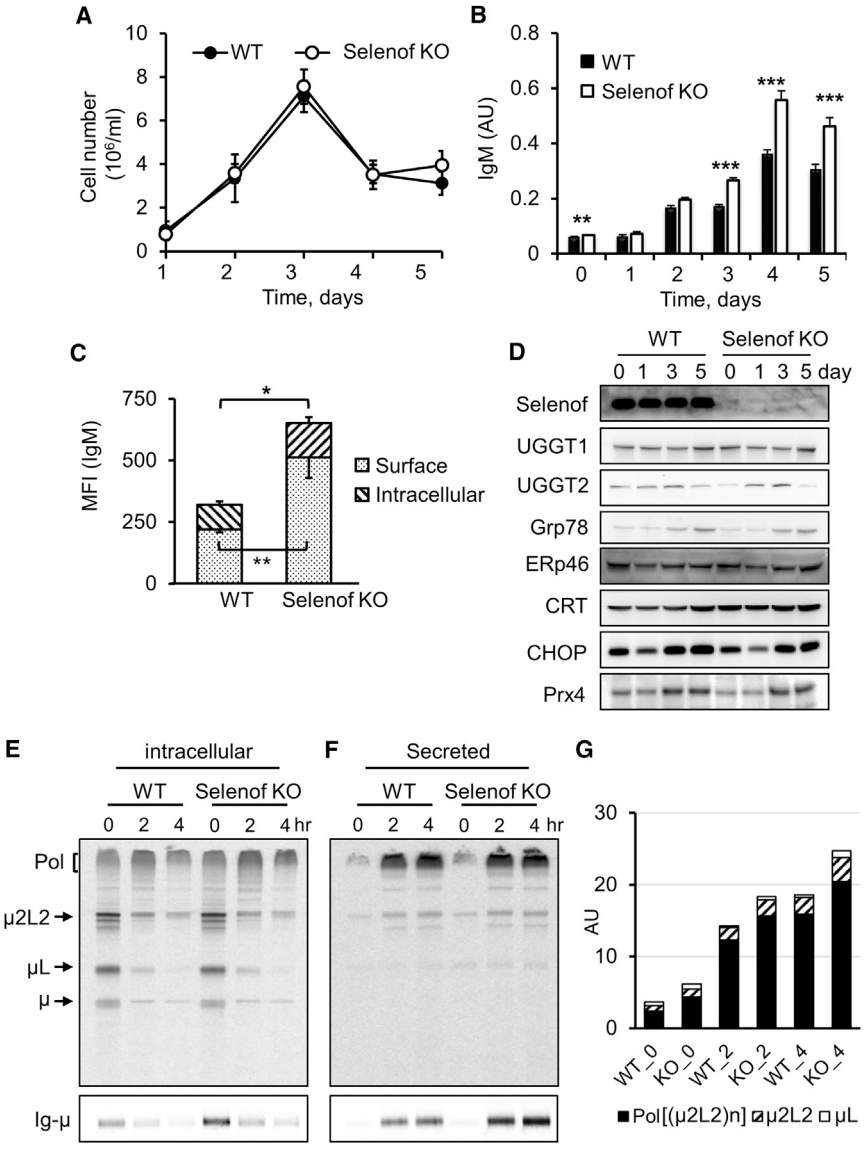

Figure 2. Elevated IgM Secretion by Selenof KO LPS-Activated B Cells

(A) Growth of LPS-stimulated B splenocytes isolated from WT and Selenof KO mice. The graph shows B cell growth during differentiation.

(B) IgM secretion measured during plasma B cell differentiation by ELISA. Two-tailed probability values of a Student's t test from day 0 to day 5 are as follows: day 0, $p = 0.0091$; day 1, $p = 0.3891$; day 2, $p = 0.18$; day 3, $p = 5E{-}06$; day 4, $p = 0.0003$; and day 5, $p = 0.0013$.

(C) Surface and intracellular IgM expression levels were measured in plasma B cells at differentiating day 4 using flow cytometry. MFI, median fluorescence intensity of the fluorescently labeled IgM.

(D) Expression of ER proteins in WT and Selenof KO B cells. Western blotting of Selenof and other ER proteins with relevance to Selenof function during B cell differentiation.

(E–G) Kinetics of IgM biosynthesis and transport were measured by radioactive pulse-chase assays (E and F) and quantified with ImageJ (G). The polymerization status of intracellular (E) and secreted (F) IgM was visualized in non-reducing conditions (E and F, upper panels), and Ig-μ levels were quantified in reducing blots (E and F, lower panels). At chase time 0, the levels of intracellular polymerization intermediates ((μ2L2)n) were increased by ~20%, and the Ig-μ levels were ~50% only slightly higher in Selenof KO plasma cells. Secreted IgM was more abundant (30–45%) in the spent media of Selenof KO LPS-activated splenocytes during the chase.

Data are expressed as mean ± SD. *$p < 0.05$; **$p < 0.01$; ***$p < 0.001$.

Selenof KO mice (n = 8 per group, 12-week-old mice), we found that Selenof deficiency leads to elevated levels of IgM in serum ($p = 0.0002$), based on ELISAs (Figure 1B). Analysis of IgM components by western blotting under reducing (Figure 1C) and non-reducing conditions (Figure 1D) revealed higher levels of both Ig-μ and Ig-k chains in the serum of Selenof KO mice. In addition, global analyses of Ig abundance showed increased levels of IgG2a, IgG2b, IgG2c, IgG3, and IgM in Selenof KO mouse serum (n = 8 per group) (Figure 1E). In contrast, serum protein levels and their patterning, as analyzed by SDS-PAGE, were not different between WT and Selenof KO mice (Figure S1), suggesting that Selenof deficiency preferentially leads to elevation of serum Igs and possibly other proteins.

Complete blood count (CBC) using Hemavet Systems showed that all 24 measured and reportable CBC parameters, except platelet count, were not different between WT and Selenof KO animals (n = 10 per group, 12-week-old male mice). Platelet counts of Selenof KO mice were approximately 20% lower than those of WT littermates ($p < 0.01$). In addition, flow-cytometric analysis showed that the proportion of splenic $CD4^+$ and $CD8^+$ T cells, as well as of $CD19^+$ B cells, were not altered by Selenof deficiency (Figure S2). Overall, the data suggested that Selenof deficiency increases Ig levels but does not lead to recognizable systemic changes in protein abundance or immune defects.

Selenof Deficiency Leads to Elevated Secretion of IgM during Plasma B Cell Differentiation

High Ig levels in the serum of Selenof KO mice may be the result of elevated production and/or decreased degradation of Igs. To characterize how Selenof deficiency alters serum IgM levels, we analyzed the rate of IgM secretion by activated plasma B cells. The proliferation rate of B cells, determined by the total number of cells per milliliter of media, during plasma B cell differentiation upon lipopolysaccharide (LPS) stimulation, was not affected by Selenof deficiency (Figure 2A). Without LPS stimulation, IgM secretion by naive B cells was higher in Selenof KO mice (day 0). Upon LPS treatment, IgM was secreted at a higher level during differentiation of splenic B cells isolated from Selenof KO mice starting from differentiation day 3, and increased IgM

production continued until termination of the experiment at day 5 (Figure 2B). Using flow cytometry, expression levels of surface and intracellular IgM were measured. Activated B cells, 4 days after the LPS treatment, showed significantly higher levels of surface IgM and intracellular IgM in the absence of Selenof compared to controls (WT cells) (Figure 2C). To determine whether Selenof deficiency and the resulting excess IgM secretory phenotype resulted in increased ER stress or altered levels of ER stress-associated proteins during plasma B cell differentiation, we analyzed relevant protein expression by western blotting (Figure 2D). Selenof expression did not change in WT B cells during differentiation, and, as expected, this protein was not detected in KO cells. The expression of UGGT1 and UGGT2 proteins, which are the binding partners of Selenof, also was not affected, and Selenof deficiency did not alter their expression. As expected, ER stress response markers GRp78 and CHOP and the antioxidant Prx4 increased, but Selenof deficiency did not modify their expression patterns. In addition, no clear changes were observed in the expression of ERp46 and calreticulin (CRT). Thus, Selenof deficiency resulted in elevated IgM secretion but did not lead to (or change the level of) ER stress during B-to-plasma cell differentiation.

Next, we evaluated the kinetics of IgM synthesis and secretion during the course of B cell differentiation at day 3 by pulse-chase analyses (Figures 2E–2G and S3). Primary B splenocytes isolated from WT and Selenof KO mice were pulse-labeled with ^{35}S-labeled amino acids, washed, and chased for 0, 2, or 4 hr. The total cell lysates (Figure S3A) or immunoprecipitates (Figures 2E and 2F) were resolved by SDS-PAGE under non-reducing (Figures 2E and 2F, upper panels) or reducing (Figures 2E and 2F, lower panels) conditions, visualized by autoradiography, and quantified with ImageJ (Figure 2G). Both intracellular (Figure 2E) and secreted (Figure 2F) IgM levels were higher in Selenof KO B cells. Secreted IgM polymers were quantified from the non-reducing SDS-PAGE (Figure 2G). Intracellular and secreted polymerized IgM ((μ2L2)n) levels were increased by 20% at 2 hr of chase in Selenof KO B cells, compared to WT controls. In addition, intracellular Ig-μ was measured under reducing SDS-PAGE conditions and found to be increased 50% at time 0 in Selenof B cells, and the levels of secreted Ig-μ were increased 25–45% during different chase time points (Figures 2E and 2F, lower panels, and S3B and S3C). These findings further support the selective elevated secretion of Igs as a consequence of Selenof deficiency.

Increased Ig Levels in Selenof KO Mice Are Not Associated with Increased Phagocytosis and Bacterial Killing Potential

We considered the possibility that elevated Igs in Selenof KO mice might be functional and might better protect mice from antigen challenges such as bacterial infection. Since a complete blood test and lymphocyte levels of Selenof KO mice were not indicative of major changes in the immune function (Figure S2), we used a mouse model of acute peritoneal inflammation to examine Ig-neutrophil-mediated bacteria killing. We challenged Selenof KO and WT mice *in vivo* by intraperitoneal *E. coli* injection and performed *in vitro* assays using *E. coli* and *S. aureus* opsonized with sera obtained from WT and Selenof KO mice and then phagocytosed by neutrophils isolated from WT animals. Additionally, pHrodo Red *E. coli* bioparticles were opsonized with WT or Selenof KO sera and tested in phagocytosis assays.

The sera from WT and Selenof KO mice were equally efficient in opsonizing, leading to the killing of both tested bacterial strains (Figure 3A). If anything, the Selenof KO serum appeared to be less efficient, rather than more efficient, in clearing *E. coli* than the WT serum, although this effect did not reach statistical significance. *In vivo* clearance of bacterial infection was also not different between WT and Selenof KO mice (Figure 3B), but again, Selenof KO mice cleared the *E. coli* infection slightly less efficiently than control mice, although this difference was not statistically significant. In addition, bioparticles with a pH-sensitive fluorophore were used to quantify particle uptake by primary B cells or macrophages after opsonization with sera from WT or Selenof KO mice. As the bioparticles turn red after internalization, we used flow cytometry to quantify the number of cells that successfully ingested bioparticles, and we detected no significant differences between the sera from WT and Selenof KO mice (Figure 3C).

To further test the functionality of antibodies in WT versus Selenof KO sera, we immunized WT and KO animals with the model antigen NP-OVA (4-hydroxy-3-nitrophenylacetyl hapten conjugated [NP] to ovalbumin protein [OVA]) and determined the amount of total as well as NP-specific IgM and IgG antibodies. Selenof KO mice had significantly higher levels of total IgM and IgG in comparison of the control mice. The amounts of NP-specific IgM and IgG antibodies, however, were significantly reduced in Selenof KO mice (Figure 3D). Overall, the data showed that elevated Ig levels in Selenof KO mice did not result in elevated clearance of bacterial infection or phagocytosis of pathogenic bioparticles *in vivo*. An *in vitro* bacterial killing assay further confirmed that this might not be due to the killing capacity of neutrophils of Selenof KO mice. Taken together, these data suggest that the excess of antibodies present in the sera of Selenof KO mice confer no obvious advantage in the functional assays utilized.

Selenof-Deficient Cells Are Not More Vulnerable to ER Stress but Show Changes Associated with ER-to-Golgi Transport

Since protein synthesis and secretion are linked to ER function (the compartment where Selenof resides), we further examined Selenof expression in mouse tissues in comparison with other proteins relevant to its function. Selenof was expressed in various organs, with the highest levels in the pancreas and brown adipose tissue (Figure 4A). A somewhat similar pattern was observed for UGGT2, whereas UGGT1 was expressed at high levels across mouse tissues.

We further developed MEFs from WT, Selenof heterozygous, and Selenof KO littermate mice and examined how protein expression is altered in these cells in response to ER stress. All examined ER stressors-thapsigargin (Figure 4B), tunicamycin (Figure 4C), and brefeldin A (Figure 4D)-induced abundant expression of GRp78/BiP and CHOP but not of UGGT1 and calreticulin. Brefeldin A (0.5 μM and 5 μM) and thapsigargin (5 nM and 50 nM) treatment reduced the expression of Selenof more than tunicamycin (50 ng/mL and 500 ng/mL). Thus, Selenof

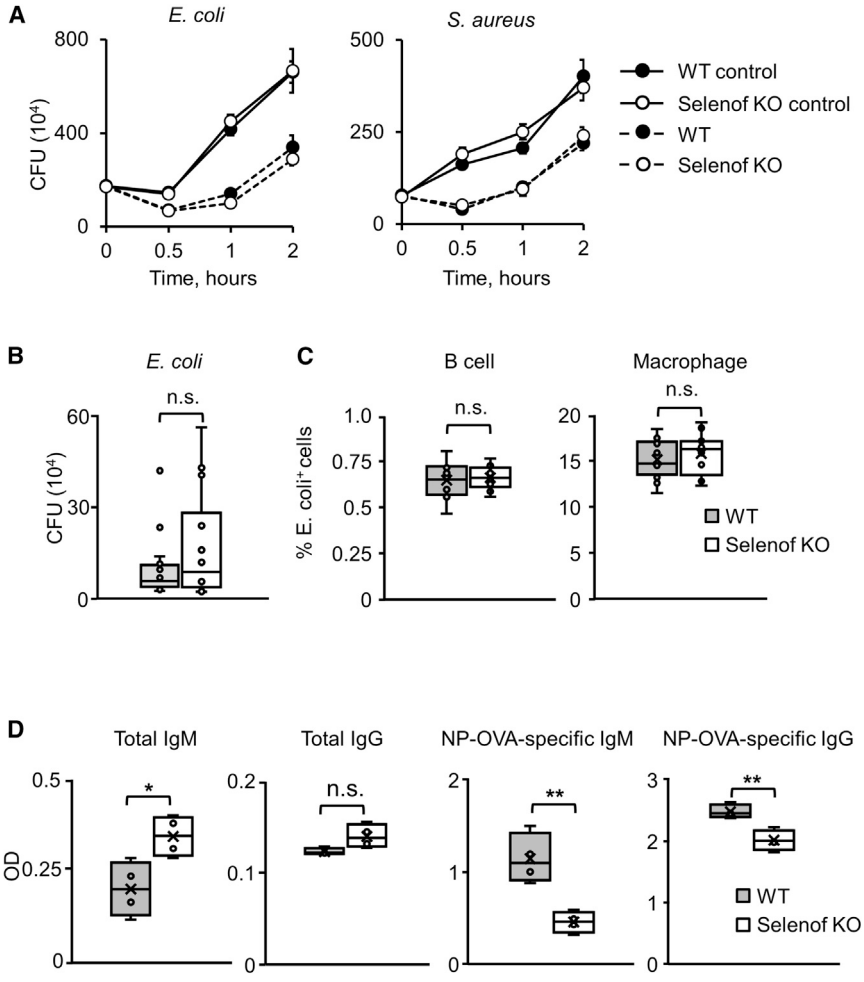

Figure 3. Elevated Immunoglobulins in Selenof Deficiency Are Partially Nonfunctional

(A) *In vitro* clearance of bacterial cells by WT and Selenof KO serum. Shown are data for *E. coli* (left) and *S. aureus* (right).

(B) *In vivo* clearance of bacterial infection by WT and Selenof KO mice. *In vivo* killing of *E. coli* by WT and Selenof KO mice, assessed as the number of remaining *E. coli* cells.

(C) Uptake of pHrodo *E. coli* bioparticles by B cells (left) and macrophages (right) from WT mice that were opsonized by WT or Selenof KO serum.

(D) Total and NP-specific IgM and IgG antibody production in WT or Selenof KO mice after immunization with NP-OVA.

Data are expressed as mean ± SD. *p < 0.05; **p < 0.01; n.s., not significant.

is not a part of the canonical, chemical-induced ER stress response pathway but may be involved in later steps of protein synthesis and trafficking, such as ER-to-Golgi transport.

To further examine the role of Selenof in ER-to-Golgi transport, an *in vivo* transport assay using the temperature-sensitive variant of VSVG protein (ts045-VSVG)-EGFP was performed (Hirschberg et al., 1998; Vanhoutte et al., 2016). WT, heterozygous (Het), and Selenof KO MEFs were transduced with the ts045-VSVG-EGFP-expressing adenovirus, and the fluorescence intensity of VSVG in whole cells and the ER-to-Golgi positive area was measured. Expression of VSVG in MEFs was synchronized prior to the VSVG crossing the Golgi by compartment progression. We found that the transport vesicles exiting the ER and trafficking to the ER-to-Golgi intermediate compartment (ERGIC) were delayed in Selenof KO MEFs, compared to WT cells (Figures 5A and 5B). Ten min after the cells shifted from non-permissive temperature to 32°C, VSVG trafficking in Selenof KO MEFs was delayed approximately 20% ($p < 0.01$), compared to WT cells. It is possible that the delayed complete clearance of the VSVG in Selenof KO MEF is a consequence of the abundant VSVG that is partially misfolded. These findings support the notion that Selenof plays a role as a gatekeeper and is involved in protein folding and sorting, and ER-to-Golgi transport.

Because Selenof KO animals were characterized by mild splenomegaly (Figure 1A), we also analyzed gene expression changes in this organ, followed by Ingenuity Pathway Analysis (IPA). Comparison of Selenof KO mice and WT littermate controls revealed several IPA "associated diseases and biofunctions" that included the categories "metabolism of protein" (198 molecules), "synthesis of protein" (91 molecules), "catabolism of protein" (121 molecules), and "ER stress response" (42 molecules, *Z* score: −0.887; $p = 0.00002$) (Data S1). Among the gene changes that contributed, the top canonical pathway identified within the ER stress response related to the "unfolded protein response." These findings support the role of Selenof in ER functions.

Inducers of ER stress, such as nutrient starvation, lead to the accumulation of unfolded proteins within the ER lumen and affect the ER-to-Golgi secretory pathway. Energy deprivation blocks the Golgi complex and the trans-Golgi network through a response mainly triggered by impaired coat protein-1 (COPI)-dependent retrograde transport from the Golgi to the ER (Chen et al., 2014). Hence, we tested whether Selenof impacted the ER-to-Golgi secretory pathway under conditions of ER stress induced by serum starvation (Figure S4). Quantitative global proteomic analyses in WT and Selenof KO MEFs were carried out, and the associated biological pathways were evaluated (Data S2). A total of 7,467 proteins were quantified by tandem mass spectrometry (MS/MS) in MEFs maintained in a serum-free culture condition. At a p value of < 0.05, 198 proteins were found to be decreased and 138 proteins increased ($n = 3$) in Selenof KO MEFs. The differentially expressed proteins ($p < 0.05$) were further analyzed and visualized using Reactome, STRING, and DAVID. Proteins decreased in Selenof KO cells (Figure 6A) were associated with "membrane part" (Gene Ontology

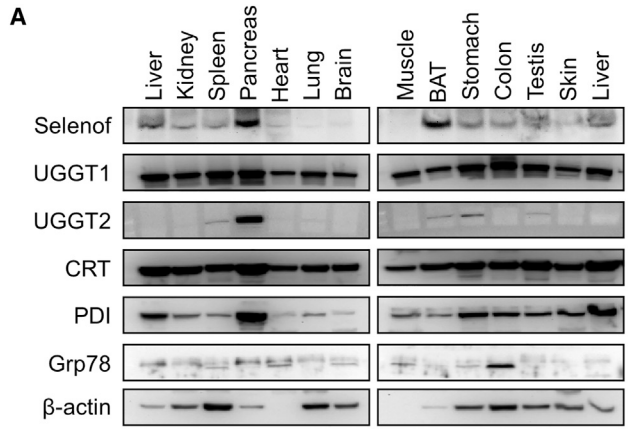

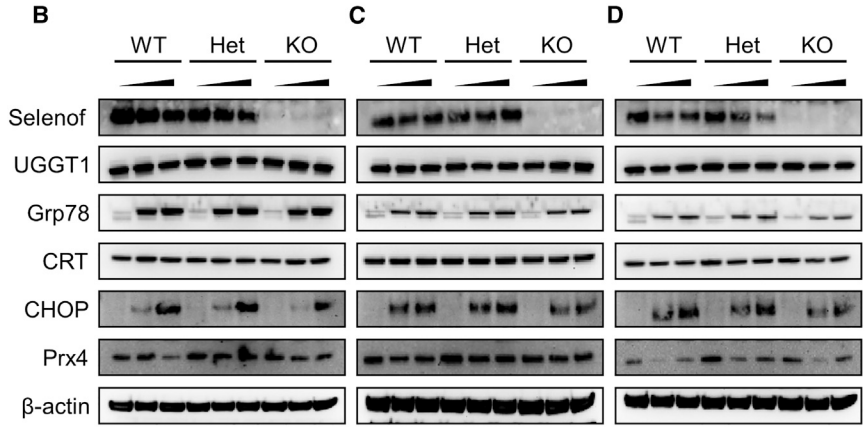

Figure 4. Selenof Deficiency Does Not Lead to ER Stress

(A) Expression pattern of Selenof and other relevant proteins across mouse tissues.

(B–D) Expression of Selenof and other relevant proteins in MEFs from WT, heterozygous, and Selenof KO mice subjected to ER stressors thapsigargin (B), tunicamycin (C), and brefeldin A (D). WT, heterozygous, and KO MEFs were treated with two concentrations of stressors along with control (DMSO treated): thapsigargin (5 nM and 50 nM), tunicamycin (50 ng/mL and 500 ng/mL), and brefeldin A (0.5 μM and 5 μM). Proteins assayed are shown on the left.

[GO]: 0011125; false discovery rate [FDR], 4.45E−17) and "regulation of cellular localization" (GO: 0032879; FDR, 9.43E−05). Seventy-three of these proteins were also associated with "catalytic activity" (GO: 0003824; FDR, 0.0004189). "Porin activity" (GO: 0015288) was also enriched (FDR, 0.000114). Proteins with elevated levels in Selenof KO MEFs were associated with several pathways, most notably with "coated vesicle membrane" (GO: 0030662; FDR, 0.000196) and "mitotic cell cycle" (GO: 0000278; FDR, 0.0194) (Figure 6B).

To examine protein-protein interactions involving Selenof and UGGT1, immunoprecipitation was performed from liver lysates of WT and Selenof KO mice using antibodies against Selenof and UGGT1, followed by MS/MS analyses (Figure S5; Data S2). The use of Selenof antibodies revealed 44 proteins ($p < 0.05$) affected by Selenof deficiency, whereas the use of UGGT1 antibodies revealed 63 proteins. Five proteins (Hsd17b4, Plec, Rpl11, Scp2, and Selenof) were detected by using both antibodies. Forty-three proteins that were enriched with Selenof antibodies were further analyzed using STRING (Figure 6C). "Structural molecule activity" was the strongest association: 17 of the 43 proteins belonged to this functional category (GO: 0005198; FDR, 3.76E−15). In addition, cellular components associated with "intermediate filament" (FDR, 5.51E−14) and "extracellular exosome" (FDR, 8.3E−08) were enriched. Other notable enriched functions were "cellular lipid catabolic process" (GO: 0044242; FDR, 0.000532), and the Kyoto Encyclopedia of Genes and Genomes (KEGG) pathway of "peroxisome" (KEGG: 04146; FDR, 2.69E−06). Among proteins differentially immunoprecipitated with UGGT1 antibodies from WT and Selenof KO livers, 30 proteins were associated with "extracellular exosome" (GO: 0070062; FDR, 3.41E−11) (Figure 6D). "Poly(A) RNA binding" (GO: 0044822; FDR, 7.21E−06) was also enriched. The Reactome-enriched biological pathways included "antigen presentation: folding, assembly, and peptide loading," "COPII (Coat Protein 2)-mediated vesicle transport," and "ER-to-Golgi transport and its associated pathways," such as vesicle transport and ER-phagosome pathway (Tables 1, S1, S2, and S3). The DAVID functional annotation tool similarly identified pathways associated with the ER to the trans-Golgi network (Table S3), including "Golgi vesicle transport" (p = 4.20E−05), "cytoplasmic membrane-bounded vesicle" (p = 1.10E−04), and "membrane-bounded vesicle" (p = 1.70E−04).

DISCUSSION

Selenof has been an enigmatic protein, many efforts to address its function notwithstanding (Hu et al., 2001; Kasaikina et al., 2011; Kumaraswamy et al., 2002; Labunskyy et al., 2005; Novoselov et al., 2006). Being a selenoprotein with a thioredoxin fold, and having Sec in the position of the redox-active Cys in thioredoxin, Selenof was expected to function as a thiol oxidoreductase. Its redox potential is −225 mV, which is between that of thioredoxin (−270 mV) and protein disulfide isomerase (−175 mV); therefore, Selenof is likely to act as a reductase or isomerase (Ferguson et al., 2006). All functionally characterized selenoproteins are oxidoreductases and the majority of thioredoxin-fold proteins are oxidoreductases. Selenof is localized in the ER due to its strong binding to UGGTs, whose function is to maintain glycoprotein quality control in the ER. Upon binding

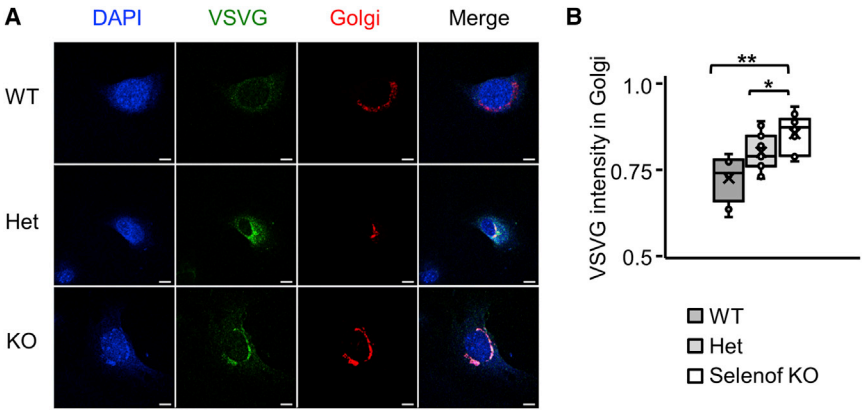

Figure 5. Delayed ER-to-Golgi Trafficking in Selenof KO MEFs

(A) Immunofluorescence micrographs of WT, heterozygous, and Selenof KO MEFs expressing adenoviral ts045-VSVG-EGFP and a Golgi marker. Representative images show the overlapping area where the VSVG-EGFP is retained in the ER-to-Golgi area, 10 min after the cells were transferred from the restrictive temperature (40°C) to the permissive temperature (32°C). Scale bars: 10 μm. (B) Quantification of VSVG fluorescence retained in the ER-to-Golgi area. Three cell lines per each genotype and more than 10 cells per each field were evaluated. Immunofluorescence microscopy images were analyzed by ImageJ. *$p < 0.05$; **$p < 0.01$.

of Selenof to UGGT1 or UGGT2, the glucosyltransferase activities of these proteins are increased (Takeda et al., 2014). Together with the previously described oxidative stress-like phenotypes that characterize Selenof deficiency in cell culture and animal models (Ferguson et al., 2006; Kasaikina et al., 2011), a possible function of Selenof was thought to be related to redox quality control of UGGT targets. However, it was difficult to examine this function.

Our findings support the idea that Selenof participates in the complex secretome gatekeeping function, likely assisting newly synthesized glycoproteins as they exit the ER or during their trafficking between the ER and the Golgi. While mice lacking Selenof are viable and fertile and have no gross morphological abnormalities, Selenof deficiency led to elevated levels of serum Igs-in particular, IgM-as well as to mild splenomegaly. We found that the elevated serum IgM levels were due to increased secretion of these molecules. The data further suggest that Selenof is a gatekeeper of UGGT targets translocated from the ER to the Golgi apparatus.

Secreted disulfide-rich proteins are characterized by a high rate of incorrect disulfide formation, as well as significant variation in glycosylation (Buchberger et al., 2010; Sevier and Kaiser, 2002). Although the calnexin-calreticulin-ERp57 system permits incorrectly glycosylated proteins to pass through an additional round of maturation (Anelli and Sitia, 2008), it has been unclear how the disulfide quality control is maintained during this process, since many UGGT clients are rich in disulfides. Selenof nicely fits this role, although it may not be the exclusive oxidoreductase in this process. It appears that Selenof deficiency weakens glycoprotein redox quality control, allowing some glycoproteins with incorrect disulfides to be secreted. If so, a subset of secreted disulfide-rich glycoproteins may bypass the checkpoint, and the secreted pool would consist of a mixture of functional and non-functional molecules. In the absence of Selenof, the latter would bypass also the ERp44 quality control system that operates beyond the ER in a pH-dependent way (Anelli et al., 2015).

Our findings support this model. While the levels of IgM, a highly glycosylated molecule with numerous inter- and intra-disulfide bridges, were elevated in Selenof KO mice, *in vitro* and *in vivo* clearance of bacterial infection was not affected. The fact that Selenof deficiency does not lead to measurable ER stress is also consistent with this possibility. In addition, Selenof protein expression was decreased upon brefeldin A and thapsigargin treatments that inhibit ER-to-Golgi transport and induce retrograde protein transport between these compartments. Also, confocal images of ts045-VSVG-EGFP-expressing MEFs confirmed that the VSVG-EGFP cargo exiting from the Golgi apparatus was delayed but, ultimately, could be completed in Selenof KO cells. Newly synthesized, secreted non-functional glycoproteins would pass through the ER and Golgi in the absence of Selenof, so the ER compartment itself would be subjected to similar levels of stress in WT and Selenof KO cells. It is unclear whether elevated levels of non-functional Igs directly cause splenomegaly, as this phenotype may also result from other processes, but at least this phenotype is consistent with the predicted function of Selenof. Nutrient-starvation-induced ER stress leads to the accumulation of unfolded proteins within the ER lumen and affects the ER-to-Golgi secretory pathway. Regulatory mechanisms preventing secretion of dysfunctional proteins from cells may be complex and involve multiple proteins or even pathways. Perturbations of ER homeostasis mediate ER stress through translational attenuation, upregulation of the ER chaperone functions, and degradation of misfolded proteins. It is also possible that some of the changes observed in Selenof KO mice are an outcome of the ER-stress-associated secondary or feedback mechanisms. Our quantitative microarray analyses in spleen indicated various mechanisms related to ER stress and protein synthesis affected by systemic Selenof deficiency in mice. Quantitative global proteomic analyses revealed that proteins differentially expressed between WT and Selenof KO MEFs were primarily enriched in the pathways associated with the ER-to-Golgi transport. Proteins that were differentially expressed and involved in antigen presentation and vesicle transport categories included Sec23a, Sec24d, Sec16b, Sec23ip, Uso1, Rab1b, and Mr1. These findings support the idea that Selenof functions as a gatekeeper and that disruption of this gene significantly affects the critical ER-to-Golgi transition.

Most previous research on thiol oxidoreduction in the ER dealt with the formation of disulfide bonds, whereas the redox gatekeeper function remained poorly characterized. Nevertheless,

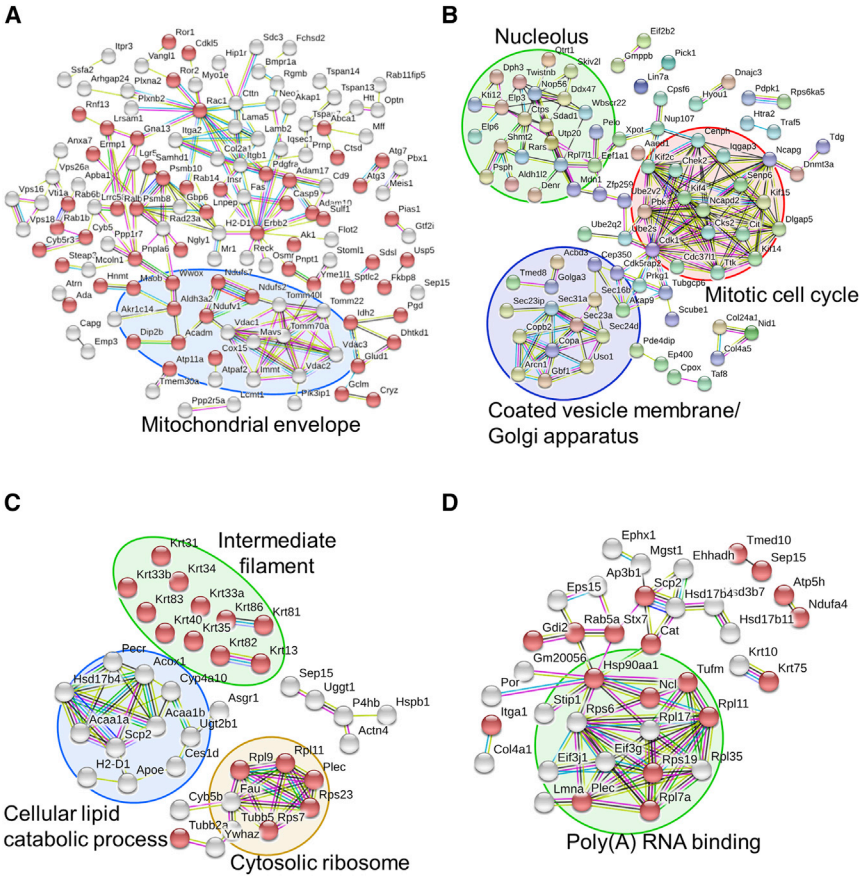

Figure 6. Network Analysis of Enriched Pathways and Interactions

(A and B) WT and Selenof KO MEFs were cultured in serum-free media and subjected to quantitative proteomics analysis. Enriched proteins ($p < 0.05$, 138 up- and 198 down-regulated in Selenof KO) were further analyzed and visualized with STRING. Proteins with catalytic activity are marked with red bubbles. The functions "membrane part" and "regulation of cellular localization" were the most decreased in Selenof KO cells. Mitochondrial envelope proteins were decreased in Selenof KO (A). Proteins with increased levels in Selenof KO MEFs belonged to the clusters "Coated vesicle membrane/Golgi apparatus" (circled in purple), "Nucleolus" (circled in green), and "Mitotic cell cycle" (circled in red) (B).

(C and D) Selenof and UGGT1 interacting proteins and the associated enriched pathways. Proteins from WT and Selenof KO livers were immunoprecipitated with antibodies against Selenof (C) or UGGT1 (D), followed by MS/MS analysis. Proteins identified ($p < 0.05$) were further analyzed. Selenof antibodies enriched 44 proteins belonging to "structural molecule activity" (marked with red bubbles). Four protein clusters were identified and visualized: "cellular lipid catabolic process" (circled in blue), "Cytosolic ribosome" (circled in yellow), "Intermediate filament" (circled in green), and Selenof along with UGGT1 (C). UGGT1 antibodies enriched 63 proteins belonging to "extracellular exosome" (marked with red bubbles). A cluster with a function "Poly(A) RNA binding proteins" is circled in green in (D). Disconnected nodes are not shown.

this function is expected to be selected during evolution (Sun et al., 2014), particularly with regard to secreted disulfide-rich proteins, as otherwise organisms would need to invest large amounts of energy in producing and then detecting and degrading secreted non-functional molecules. The gatekeeper function of Selenof is likely not limited to IgM or, more generally, to Igs. Selenof is expressed in all cells and appears to target a subset of secreted proteins. It is possible that the phenotype we observed in activated B cells was better exposed due to the specialized function of these cells in secreting large quantities of disulfide-rich glycoproteins.

Our work was performed using mouse models, which tolerate Selenof deficiency and exhibit relatively mild phenotypes, at least in the lab setting. Interestingly, based on the analysis of more than 60,000 human exomes (http://exac.broadinstitute.org/) (Lek et al., 2016), we found that the loss-of-function SELENOF alleles (functionally equivalent to heterozygous KO) are depleted 5-fold compared to the expected occurrence, whereas the occurrence of synonymous and missense mutations in SELENOF is as expected. This observation suggests that the SELENOF-supported function may be more important in long-lived humans than in short-lived mice. Selenof has a paralog, Selenom, in both mice and humans, and it is also a selenoprotein. However, Selenom does not bind UGGTs or increase the activity of UGGTs (Ito et al., 2015; Takeda et al., 2014). We speculate that it may serve some other subsets of disulfide-containing proteins that pass through the ER.

Overall, this study identifies a new function of the selenoprotein oxidoreductase Selenof: a gatekeeper of secreted disulfide-rich glycoproteins. The data suggest that it blocks these proteins from secretion when they possess incorrectly formed disulfides or have some other redox-related errors in their Cys residues that inhibit their functions, so the erroneous proteins are subjected to additional rounds of maturation in the ER.

EXPERIMENTAL PROCEDURES

Materials

Tunicamycin, brefeldin A, and thapsigargin were from Tocris Bioscience (Bristol, UK); and lipopolysaccharide (LPS; L2637), SIGMAFAST OPD (o-phenylenediamine), and 2-mercaptoethanol were from Sigma (St. Louis, MO, USA). Cell culture media (DMEM and RPMI), antibiotics, non-essential amino acids, sodium pyruvate, N-glutamine, insulin-transferrin-selenium (ITS-G, 100×), serum, and ammonium-chloride-potassium (ACK) lysis buffer were from Invitrogen. For western blot analysis, NuPAGE 10% Bis-Tris and NativePAGE 4–16% Bis-Tris Gel systems (Invitrogen) were used. The following antibodies for western blotting were used: anti-β-Actin (Sigma), anti-Selenof (NCIR128A, Abcam), anti-Peroxiredoxin 4 (Prx4, AbFrontier, Korea), anti-UDP-glucose:glycoprotein glucosyltransferase 1 and anti-UDP-glucose:glycoprotein glucosyltransferase 2 (UGGT1 and UGGT2, Novus Biologicals), anti-calreticulin (Cell Signaling Technology), anti-CCAAT/anti-enhancer-binding protein homologous protein (CHOP, Abcam), anti-46 kDa endoplasmic

Table 1. Pathway Enrichment Analysis of 336 Proteins Differentially Expressed between Selenof KO and WT Mouse Embryonic Fibroblast Cells

Pathway	Proteins Found	Proteins Total	Ratio	p Value	FDR
Antigen presentation: folding, assembly, and peptide loading of class I MHC	14	118	0.011	1.46E−06	0.00115
Laminin interactions	6	31	0.003	1.21E−04	0.0476
COPII (Coat Protein 2)-mediated vesicle transport	8	75	0.007	5.36E−04	0.103
Endosomal/vacuolar pathway	9	97	0.009	6.60E−04	0.103
Antigen processing-cross-presentation	12	176	0.016	1.32E−03	0.162
ER-phagosome pathway	11	154	0.014	1.45E−03	0.162
Class I MHC-mediated antigen processing and presentation	18	368	0.033	3.87E−03	0.379
ER-to-Golgi anterograde transport	10	157	0.014	5.22E−03	0.407
Transport to the Golgi and subsequent modification	12	212	0.019	5.82E−03	0.414
WNT5A-dependent internalization of FZD2, FZD5, and ROR2	2	5	0	6.66E−03	0.433
Golgi cisternae pericentriolar stack reorganization	3	17	0.002	8.35E−03	0.501
Constitutive signaling by NOTCH1 t(7;9)(NOTCH1:M1580_K2555) translocation mutant	2	8	0.001	1.63E−02	0.558
Signaling by NOTCH1 t(7;9)(NOTCH1:M1580_K2555) translocation mutant	2	8	0.001	1.63E−02	0.558
Non-integrin membrane-ECM interactions	5	61	0.006	1.68E−02	0.558
Interferon alpha/beta signaling	8	138	0.013	1.97E−02	0.558
5-Phosphoribose 1-diphosphate biosynthesis	2	9	0.001	2.03E−02	0.558
CHL1 interactions	2	10	0.001	2.46E−02	0.558
Interferon gamma signaling	9	174	0.016	2.64E−02	0.558
Zinc influx into cells by the SLC39 gene family	2	11	0.001	2.94E−02	0.558
Sema4D-induced cell migration and growth-cone collapse	3	28	0.003	3.08E−02	0.558

The Reactome pathway database was used for enrichment analysis. $p < 0.05$.

reticulum protein (ERp46, Abcam), anti-glucose regulated protein 78 (GRp78, Abcam), and rabbit anti-mouse IgM antibody (cat# 61-6800, Zymed). For ELISAs, goat anti-mouse IgG1-HRP (horseradish peroxidase), goat anti-mouse IgA-HRP, goat anti-mouse IgG2a-HRP, goat anti-mouse IgG2b-HRP, goat anti-mouse IgG2c-HRP, goat anti-mouse IgG3-HRP, goat anti-mouse IgE-HRP, and anti-IgM μ-HRP were from SouthernBiotech. CellLight Golgi-RFP, BacMam 2.0, and pHrodo Red *E. coli* BioParticles were from Thermo Fisher Scientific. Mouse B cell and neutrophil isolation kits were from Miltenyi Biotec. BD Microtainer serum separator tubes were from BD Biosciences. Bacterial strains *Staphylococcus aureus* (*S. aureus*, strain 10390) and *E. coli* (*E. coli*, strain 19138) were from the American Type Culture Collection (ATCC).

Mice

Selenof KO mice were generated as previously described (Kasaikina et al., 2011) and backcrossed to C57BL/6J background for at least 10 generations. WT and Selenof KO mice for the described experiments were produced by mating heterozygous animals. Genotyping was performed by PCR using Selenof gene-specific primers (forward [F]1: GCA GCT CTT GCG ATC TTC TT and reverse [R]1: TTT GGC CAG ATA CCA GGA AG) and inserted Neo-cassette specific primer (F2: TCG CCT TCT TGA CGA GTT CT). Littermate male mice, aged 8 to 14 weeks, were used for all experiments, except for the generation of Selenof MEF cells. Experimental animal protocols were approved by the Institutional Animal Care and Use Committees of Brigham and Women's Hospital, Harvard University, and University of Nebraska-Lincoln.

Generation of MEFs and Cell Culture

Primary MEFs were generated by mating Selenof heterozygous animals. Pregnant females were sacrificed on day 13.5 post-coitum, embryos were surgically removed, and fibroblast cells were prepared in culture. Each embryo was cultured separately and was genotyped for the disruption of the Selenof gene. Selenof WT, heterozygous, and KO cells were generated from a single litter, and same-passage cells were used for the study. MEFs were cultured in DMEM (Invitrogen) supplemented with 1 mM non-essential amino acids, 10% fetal bovine serum, 1% penicillin-streptomycin (Pen/Strep), and 0.5 μmol/L 2-mercaptoethanol (β-ME). MEFs used in the experiments were in passages 3 to 7 without immortalization.

Selenof WT, heterozygous, and KO MEF cells were treated with ER-stress-inducing agents. For tunicamycin (TM), brefeldin A (BFA), and thapsigargin (TG) treatments, 1,000× stock solutions were prepared in DMSO, and an equal volume of DMSO alone (0.1%, v/v) was applied to cell culture as a control. MEF cells (WT, heterozygous, and KO) derived from a single litter and same passage number were plated at a concentration of 10^6 cells per 10-cm dish and allowed to attach overnight prior to application of ER-stress-inducing reagents. The cells were treated with tunicamycin (50 ng/mL or 500 ng/mL), TG (5 nM or 50 nM), brefeldin A (0.5 μM or 5 μM), or DMSO (0.1%, v/v). After 24 hr of treatment with ER-stress-inducing agents, cell culture plates were briefly washed twice with ice-cold PBS, and the attached cells were directly lysed with SDS sample buffer for protein analysis.

Liquid Chromatography-Tandem Mass Spectrometry Analysis and Pathway Enrichment Analysis

To subject cells to serum starvation, MEFs derived from littermate embryos (three WT and three Selenof KO) were seeded in 150-mm dishes for 24 hr and washed twice in PBS, and the culture media were replaced with phenol-red-free RPMI 1640 media supplemented with insulin-transferrin-selenium (1 g/L, 0.55 g/L, and 0.67 mg/L as sodium selenite, respectively). Three days later, adherent cells were lysed in ice-cold protein lysis buffer (50 mM HEPES [pH 7.5], 150 mM KCl, 2 mM EDTA, 1 mM NaF, 0.5% [v/v] NP-40, 0.5 mM DTT, and protease inhibitor cocktail [Roche, EDTA-free], and 10 mM N-ethylmaleimide). After enzymatic digestion, an aliquot of

100 μg peptide per condition was fractionated and then analyzed by liquid chromatography-tandem mass spectrometry (LC-MS/MS) using an Orbitrap Fusion Lumos (Thermo Fisher Scientific). Mass-spectrometry data were searched using Sequest and filtered to a 1% FDR at the protein level to generate the target protein list. Proteins that are differentially expressed with a p value less than 0.05 between Selenof WT and KO MEFs were further analyzed for pathway enrichment. Protein interaction databases Reactome (Fabregat et al., 2016), STRING (Szklarczyk et al., 2017), and DAVID (Huang et al., 2009) were used for network analyses. In a separate experiment, immunoprecipitation (IP) was performed from livers of WT and Selenof KO with antibodies against Selenof or UGGT1. Livers were perfused with PBS to remove blood prior to tissue collection. Antibodies were first conjugated to magnetic beads to prevent co-elution using a Dynabeads Antibody Coupling Kit prior to performing IP. Proteins eluted using each antibody were subjected for MS/MS analysis for protein identification and quantification.

Splenic B Cell Isolation and Differentiation

Spleens of WT and Selenof KO mice were removed aseptically and mashed through cell strainers. The splenocytes were prepared by lysing red blood cells using ACK lysis buffer. Splenic B cells were further purified by magnetic isolation with a mouse B cell isolation kit by depletion of non-B cells (Miltenyi Biotec) (Bertolotti et al., 2010). Pre-splenic B cells of WT and Selenof KO mice at a concentration of 2×10^6 cells per milliliter were cultured in a flask with RPMI medium containing 10% endotoxin-free fetal calf serum, 100 U/mL penicillin/streptomycin, 1 mM sodium pyruvate, 2 mM *N*-glutamine, and 50 μM β-ME. Primary B cells were activated by the addition of 20 μg/mL LPS in culture media. Daily, a one-third volume of culture media was replaced with fresh RPMI medium containing β-ME and LPS to avoid risk of starvation or oxidative stress. A portion of the cells was harvested daily for cell count and at days 0, 1, 3, and 5 for protein analyses. Cell proliferation curves were plotted by counting putative cell numbers (per milliliter of culture media) on each day after LPS-stimulated plasma B cell activation.

Immunoglobulin Production Assay

Secreted IgM levels during B cell activation were measured daily using ELISA. See the Supplemental Experimental Procedures for full details.

ELISA

Analysis of antigen-specific Ig titers in serum and B cell culture media was performed with capture ELISA. See the Supplemental Experimental Procedures for full details.

Flow Cytometry

Flow cytometry was performed on an LSR II instrument (BD Biosciences), and data were analyzed using FlowJo v10.1 (FlowJo). See the Supplemental Experimental Procedures for full details.

Neutrophil Isolation for Bacteria Killing Assay

Murine bone-marrow-derived neutrophils were isolated from 12-week-old C57BL/6J WT male animals with a Neutrophil Isolation Kit (Miltenyi Biotec). See the Supplemental Experimental Procedures for full details.

In Vitro and *In Vivo* Bacteria Killing Assays

Fresh overnight cultures of *S. aureus* (ATCC strain 10390) and *E. coli* (ATCC strain 19138) were used for *in vitro* bacteria killing assays, and *E. coli* cells were used for *in vivo* assay. See the Supplemental Experimental Procedures for full details.

pHrodo Red Bead Uptake

B cells and macrophages from WT mice were purified using magnetic isolation by depleting non-B cells or positively selecting for $CD11b^+$ cells, respectively (Miltenyi Biotec). The purified cells were incubated in R10 medium with 10% sera collected from WT or Selenof KO mice, and pHrodo Red *E. coli* BioParticles were added. After 2 hr, the *in vitro* uptake of pHrodo Red beads by B cells and macrophages was determined using flow cytometry.

Mouse Immunization and NP-Specific Antibody Production

Six- to 12-week-old WT or Selenof KO mice were immunized with 100 μg NP16-OVA (Biosearch Technologies) in a 1:1 H37RA complete Freund's adjuvant (CFA; DIFCO) emulsion. The emulsion was injected subcutaneously into the left and right flanks of each experimental mouse. 14 days after immunization, NP-specific antibody titers were measured by the incubation of serum for 1 hr in ELISA plates coated with NP16-BSA (Biosearch Technologies), followed by incubation with alkaline-phosphatase-conjugated IgG-detection and IgM-detection antibodies (1030-04; SouthernBiotech). The level of activity was measured as optical density (OD) units using a Spectramax ELISA plate reader (Molecular Devices).

VSVG Transport Assay

Anterograde transport of VSVG-EGFP in WT, heterozygous, and Selenof KO MEFs was analyzed using the ts045-VSVG-EGFP (kindly provided by Dr. Jeffery D. Molkentin) as described previously (Vanhoutte et al., 2016). Briefly, 48 hr after adenoviral transduction, cells were co-infected with CellLight Golgi-RFP Bacmmam 2.0 and incubated at 40°C for 20 hr to retain the VSVG-EGFP in the ER. To measure the co-localization of VSVG-EGFP during the ER-to-Golgi transit, cells were shifted to 32°C, allowing the VSVG-EGFP to traffic to the Golgi apparatus. Three independent MEF lines per each genotype were tested. Representative confocal images of VSVG-EGFP fluorescence overlapping with Golgi-RFP were captured (n = 10 per each MEF line). Fractions of VSVG-EGFP retained in the Golgi apparatus at 10 min after being released were further analyzed. All images were captured, analyzed, and quantified with the ImageJ program (NIH), and overlapping signals were measured.

Radioactive Pulse-Chase Assay

Kinetics of IgM biosynthesis and transport were measured with a radioactive pulse-chase assay (Cals et al., 1996; Mezghrani et al., 2001) in primary B cells isolated from WT and Selenof KO mice. See the Supplemental Experimental Procedures for full details.

Statistical Analyses

Data are expressed as the mean ± SD as indicated. Two-tailed Student's t tests were used for comparing different groups of samples, and significant differences were defined as $^*p < 0.05$, $^{**}p < 0.01$, and $^{***}p < 0.001$, unless otherwise stated.

SUPPLEMENTAL INFORMATION

Supplemental Information includes Supplemental Experimental Procedures, five figures, three tables, and three data files and can be found with this article online at https://doi.org/10.1016/j.celrep.2018.04.009.

ACKNOWLEDGMENTS

We thank Drs. Davy Vanhoutte and Jeffery Molkentin for the generous gift of temperature-sensitive VSVG-EGFP adenovirus. This work was supported by NIH grant CA080946 (to V.N.G.) and AIRC IG-18624 (to R.S.).

AUTHOR CONTRIBUTIONS

Conceptualization, S.H.Y. and V.N.G.; Methodology, S.H.Y., R.A.E., and F.A.S.; Investigation, S.H.Y., R.A.E., S.-G.L., A.O., K.K., Z.R.B., F.A.S., and P.A.T.; Resources, A.H.S., S.P.G., and V.N.G.; Writing – Original Draft, S.H.Y. and V.N.G.; Writing – Review & Editing, S.H.Y., V.N.G., D.L.H., A.H.S., R.S., S.P.G., H.R.L., and D.E.F.

DECLARATION OF INTERESTS

The authors declare no competing interests.

Received: January 4, 2017
Revised: January 8, 2018
Accepted: March 31, 2018
Published: May 1, 2018

REFERENCES

Anelli, T., and Sitia, R. (2008). Protein quality control in the early secretory pathway. EMBO J. *27*, 315–327.

Anelli, T., Sannino, S., and Sitia, R. (2015). Proteostasis and "redoxtasis" in the secretory pathway: Tales of tails from ERp44 and immunoglobulins. Free Radic. Biol. Med. *83*, 323–330.

Arnold, J.N., Wormald, M.R., Sim, R.B., Rudd, P.M., and Dwek, R.A. (2007). The impact of glycosylation on the biological function and structure of human immunoglobulins. Annu. Rev. Immunol. *25*, 21–50.

Berry, M.J., Banu, L., Chen, Y.Y., Mandel, S.J., Kieffer, J.D., Harney, J.W., and Larsen, P.R. (1991). Recognition of UGA as a selenocysteine codon in type I deiodinase requires sequences in the 3′ untranslated region. Nature *353*, 273–276.

Bertolotti, M., Yim, S.H., Garcia-Manteiga, J.M., Masciarelli, S., Kim, Y.J., Kang, M.H., Iuchi, Y., Fujii, J., Vene, R., Rubartelli, A., et al. (2010). B- to plasma-cell terminal differentiation entails oxidative stress and profound reshaping of the antioxidant responses. Antioxid. Redox Signal. *13*, 1133–1144.

Buchberger, A., Bukau, B., and Sommer, T. (2010). Protein quality control in the cytosol and the endoplasmic reticulum: brothers in arms. Mol. Cell *40*, 238–252.

Cabral, C.M., Liu, Y., and Sifers, R.N. (2001). Dissecting glycoprotein quality control in the secretory pathway. Trends Biochem. Sci. *26*, 619–624.

Cals, M.M., Guenzi, S., Carelli, S., Simmen, T., Sparvoli, A., and Sitia, R. (1996). IgM polymerization inhibits the Golgi-mediated processing of the mu-chain carboxy-terminal glycans. Mol. Immunol. *33*, 15–24.

Caramelo, J.J., and Parodi, A.J. (2008). Getting in and out from calnexin/calreticulin cycles. J. Biol. Chem. *283*, 10221–10225.

Cenci, S., and Sitia, R. (2007). Managing and exploiting stress in the antibody factory. FEBS Lett. *581*, 3652–3657.

Chen, R., Zou, Y., Mao, D., Sun, D., Gao, G., Shi, J., Liu, X., Zhu, C., Yang, M., Ye, W., et al. (2014). The general amino acid control pathway regulates mTOR and autophagy during serum/glutamine starvation. J. Cell Biol. *206*, 173–182.

Dejgaard, S., Nicolay, J., Taheri, M., Thomas, D.Y., and Bergeron, J.J. (2004). The ER glycoprotein quality control system. Curr. Issues Mol. Biol. *6*, 29–42.

Ehrenstein, M.R., and Notley, C.A. (2010). The importance of natural IgM: scavenger, protector and regulator. Nat. Rev. Immunol. *10*, 778–786.

Fabregat, A., Sidiropoulos, K., Garapati, P., Gillespie, M., Hausmann, K., Haw, R., Jassal, B., Jupe, S., Korninger, F., McKay, S., et al. (2016). The Reactome pathway Knowledgebase. Nucleic Acids Res. *44* (*D1*), D481–D487.

Ferguson, A.D., Labunskyy, V.M., Fomenko, D.E., Araç, D., Chelliah, Y., Amezcua, C.A., Rizo, J., Gladyshev, V.N., and Deisenhofer, J. (2006). NMR structures of the selenoproteins Sep15 and SelM reveal redox activity of a new thioredoxin-like family. J. Biol. Chem. *281*, 3536–3543.

Frand, A.R., Cuozzo, J.W., and Kaiser, C.A. (2000). Pathways for protein disulphide bond formation. Trends Cell Biol. *10*, 203–210.

Gladyshev, V.N., Jeang, K.T., Wootton, J.C., and Hatfield, D.L. (1998). A new human selenium-containing protein. Purification, characterization, and cDNA sequence. J. Biol. Chem. *273*, 8910–8915.

Hammond, C., Braakman, I., and Helenius, A. (1994). Role of N-linked oligosaccharide recognition, glucose trimming, and calnexin in glycoprotein folding and quality control. Proc. Natl. Acad. Sci. USA *91*, 913–917.

Hatahet, F., and Ruddock, L.W. (2009). Protein disulfide isomerase: a critical evaluation of its function in disulfide bond formation. Antioxid. Redox Signal. *11*, 2807–2850.

Hendershot, L., and Sitia, R. (2005). Immunoglobulin assembly and secretion. In Molecular Biology of B Cells, T. Honjo, F.W. Alt, and M.S. Neuberger, eds. (Elsevier Academic Press), pp. 261–273.

Hirschberg, K., Miller, C.M., Ellenberg, J., Presley, J.F., Siggia, E.D., Phair, R.D., and Lippincott-Schwartz, J. (1998). Kinetic analysis of secretory protein traffic and characterization of golgi to plasma membrane transport intermediates in living cells. J. Cell Biol. *143*, 1485–1503.

Hu, Y.J., Korotkov, K.V., Mehta, R., Hatfield, D.L., Rotimi, C.N., Luke, A., Prewitt, T.E., Cooper, R.S., Stock, W., Vokes, E.E., et al. (2001). Distribution and functional consequences of nucleotide polymorphisms in the 3′-untranslated region of the human Sep15 gene. Cancer Res. *61*, 2307–2310.

Huang, W., Sherman, B.T., and Lempicki, R.A. (2009). Systematic and integrative analysis of large gene lists using DAVID bioinformatics resources. Nat. Protoc. *4*, 44–57.

Ito, Y., Takeda, Y., Seko, A., Izumi, M., and Kajihara, Y. (2015). Functional analysis of endoplasmic reticulum glucosyltransferase (UGGT): Synthetic chemistry's initiative in glycobiology. Semin. Cell Dev. Biol. *41*, 90–98.

Kasaikina, M.V., Fomenko, D.E., Labunskyy, V.M., Lachke, S.A., Qiu, W., Moncaster, J.A., Zhang, J., Wojnarowicz, M.W., Jr., Natarajan, S.K., Malinouski, M., et al. (2011). Roles of the 15-kDa selenoprotein (Sep15) in redox homeostasis and cataract development revealed by the analysis of Sep 15 knockout mice. J. Biol. Chem. *286*, 33203–33212.

Korotkov, K.V., Kumaraswamy, E., Zhou, Y., Hatfield, D.L., and Gladyshev, V.N. (2001). Association between the 15-kDa selenoprotein and UDP-glucose:glycoprotein glucosyltransferase in the endoplasmic reticulum of mammalian cells. J. Biol. Chem. *276*, 15330–15336.

Kryukov, G.V., Castellano, S., Novoselov, S.V., Lobanov, A.V., Zehtab, O., Guigó, R., and Gladyshev, V.N. (2003). Characterization of mammalian selenoproteomes. Science *300*, 1439–1443.

Kumaraswamy, E., Korotkov, K.V., Diamond, A.M., Gladyshev, V.N., and Hatfield, D.L. (2002). Genetic and functional analysis of mammalian Sep15 selenoprotein. Methods Enzymol. *347*, 187–197.

Labunskyy, V.M., Ferguson, A.D., Fomenko, D.E., Chelliah, Y., Hatfield, D.L., and Gladyshev, V.N. (2005). A novel cysteine-rich domain of Sep15 mediates the interaction with UDP-glucose:glycoprotein glucosyltransferase. J. Biol. Chem. *280*, 37839–37845.

Labunskyy, V.M., Yoo, M.H., Hatfield, D.L., and Gladyshev, V.N. (2009). Sep15, a thioredoxin-like selenoprotein, is involved in the unfolded protein response and differentially regulated by adaptive and acute ER stresses. Biochemistry *48*, 8458–8465.

Labunskyy, V.M., Hatfield, D.L., and Gladyshev, V.N. (2014). Selenoproteins: molecular pathways and physiological roles. Physiol. Rev. *94*, 739–777.

Leijh, P.C., van den Barselaar, M.T., van Zwet, T.L., Daha, M.R., and van Furth, R. (1979). Requirement of extracellular complement and immunoglobulin for intracellular killing of micro-organisms by human monocytes. J. Clin. Invest. *63*, 772–784.

Lek, M., Karczewski, K.J., Minikel, E.V., Samocha, K.E., Banks, E., Fennell, T., O'Donnell-Luria, A.H., Ware, J.S., Hill, A.J., Cummings, B.B., et al.; Exome Aggregation Consortium (2016). Analysis of protein-coding genetic variation in 60,706 humans. Nature *536*, 285–291.

Mezghrani, A., Fassio, A., Benham, A., Simmen, T., Braakman, I., and Sitia, R. (2001). Manipulation of oxidative protein folding and PDI redox state in mammalian cells. EMBO J. *20*, 6288–6296.

Novoselov, S.V., Hua, D., Lobanov, A.V., and Gladyshev, V.N. (2006). Identification and characterization of Fep15, a new selenocysteine-containing member of the Sep15 protein family. Biochem. J. *394*, 575–579.

Reeves, M.A., and Hoffmann, P.R. (2009). The human selenoproteome: recent insights into functions and regulation. Cell. Mol. Life Sci. *66*, 2457–2478.

Sevier, C.S., and Kaiser, C.A. (2002). Formation and transfer of disulphide bonds in living cells. Nat. Rev. Mol. Cell Biol. *3*, 836–847.

Sitia, R., Rubartelli, A., and Hämmerling, U. (1984). The role of glycosylation in secretion and membrane expression of immunoglobulins M and A. Mol. Immunol. *21*, 709–719.

Sousa, M.C., Ferrero-Garcia, M.A., and Parodi, A.J. (1992). Recognition of the oligosaccharide and protein moieties of glycoproteins by the UDP-Glc:glycoprotein glucosyltransferase. Biochemistry *31*, 97–105.

Spang, A. (2013). Retrograde traffic from the Golgi to the endoplasmic reticulum. Cold Spring Harb. Perspect. Biol. *5*, a013391.

Sun, H., Deng, T., and Fu, J. (2014). Chicken 15-kDa selenoprotein plays important antioxidative function in splenocytes. Biol. Trace Elem. Res. *161*, 288–296.

Szklarczyk, D., Morris, J.H., Cook, H., Kuhn, M., Wyder, S., Simonovic, M., Santos, A., Doncheva, N.T., Roth, A., Bork, P., et al. (2017). The STRING database in 2017: quality-controlled protein-protein association networks, made broadly accessible. Nucleic Acids Res. *45* (*D1*), D362–D368.

Takeda, Y., Seko, A., Hachisu, M., Daikoku, S., Izumi, M., Koizumi, A., Fujikawa, K., Kajihara, Y., and Ito, Y. (2014). Both isoforms of human UDP-glucose:glycoprotein glucosyltransferase are enzymatically active. Glycobiology *24*, 344–350.

Trombetta, E.S., and Helenius, A. (2000). Conformational requirements for glycoprotein reglucosylation in the endoplasmic reticulum. J. Cell Biol. *148*, 1123–1129.

Vanhoutte, D., Schips, T.G., Kwong, J.Q., Davis, J., Tjondrokoesoemo, A., Brody, M.J., Sargent, M.A., Kanisicak, O., Yi, H., Gao, Q.Q., et al. (2016). Thrombospondin expression in myofibers stabilizes muscle membranes. eLife *5*, e17589.

Zuber, C., Fan, J.Y., Guhl, B., Parodi, A., Fessler, J.H., Parker, C., and Roth, J. (2001). Immunolocalization of UDP-glucose:glycoprotein glucosyltransferase indicates involvement of pre-Golgi intermediates in protein quality control. Proc. Natl. Acad. Sci. USA *98*, 10710–10715.

Cell Reports, Volume *23*

Supplemental Information

Role of Selenof as a Gatekeeper of Secreted Disulfide-Rich Glycoproteins

Sun Hee Yim, Robert A. Everley, Frank A. Schildberg, Sang-Goo Lee, Andrea Orsi, Zachary R. Barbati, Kutay Karatepe, Dmitry E. Fomenko, Petra A. Tsuji, Hongbo R. Luo, Steven P. Gygi, Roberto Sitia, Arlene H. Sharpe, Dolph L. Hatfield, and Vadim N. Gladyshev

SUPPLEMENTAL INFORMATION

Supplemental Figures

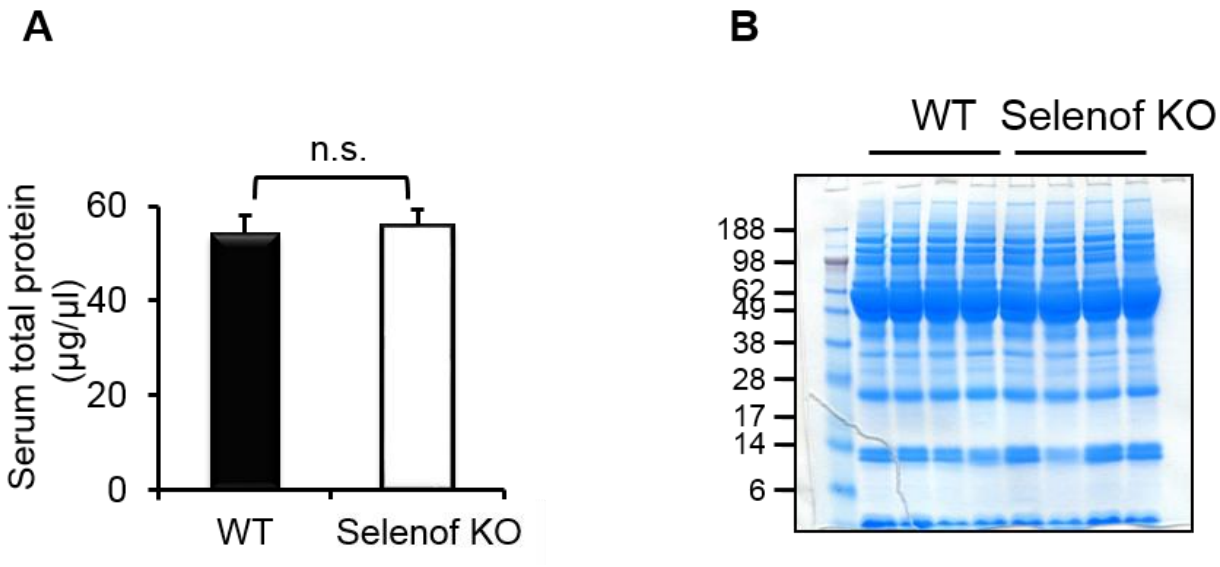

Figure S1. Selenof deficiency does not affect protein levels in plasma, related to Fig. 1. (A) Total protein in the sera of WT and Selenof KO mice. The serum protein concentration of WT mice was 54.2±3.81 μg/ul and Selenof KO was 55.81±3.39 μg/ul (p=0.32, n=10 per group). (B) Protein staining of the sera from WT and Selenof KO mice analyzed by SDS-PAGE.

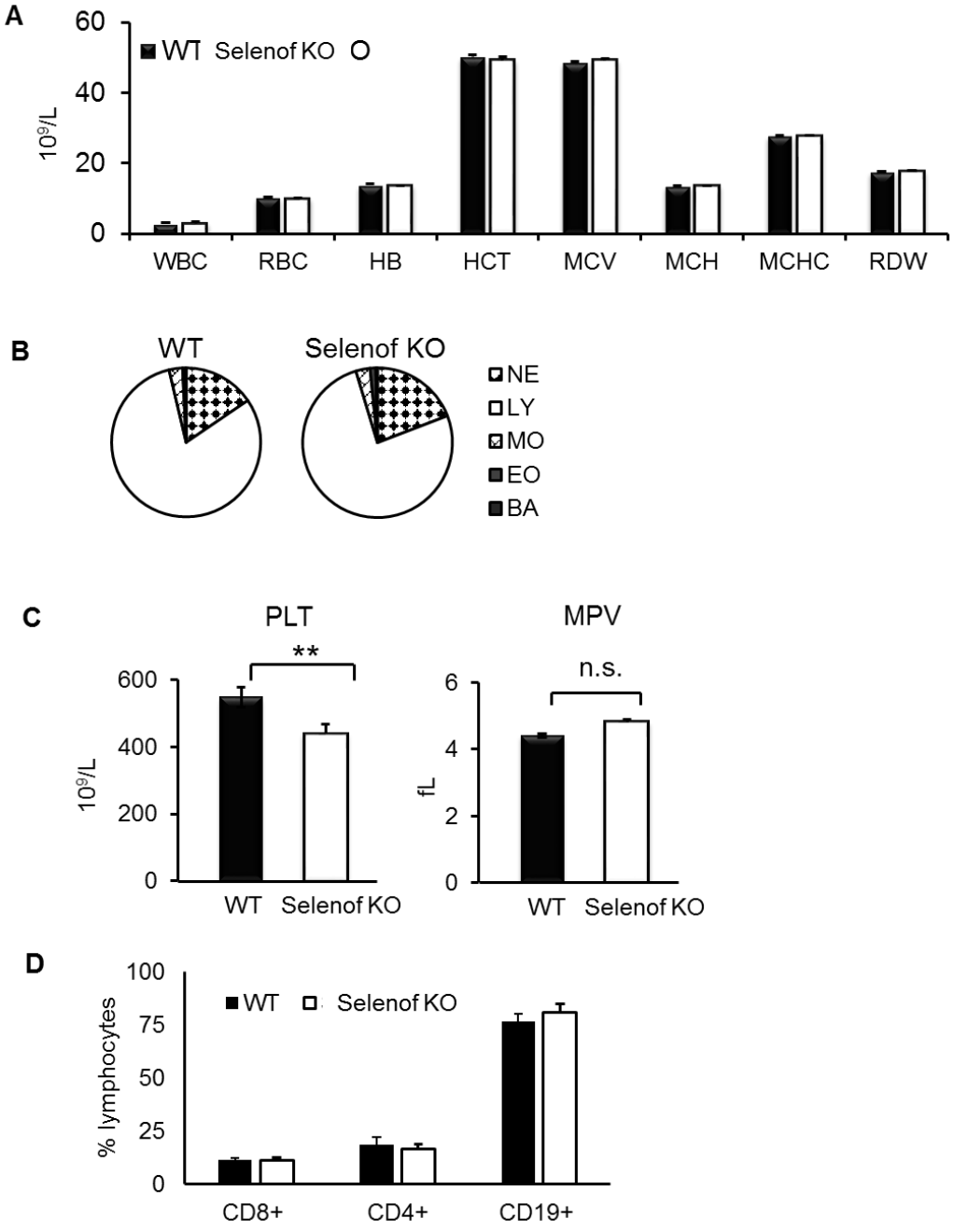

Figure S2. Selenof deficiency leads to a decrease in platelet count, related to Fig. 1. (A) Complete blood analyses using Hemavet Systems are shown for WT and Selenof KO mice (n=10 per group, 12-week-old male mice), including (B) neutrophils (polys and bands) (NE); lymphocytes (LY); monocytes (MO); eosinophils (EO); and basophils (BA). Units of measurement: (A) WBC (total white blood cells, K/μL), RBC (total red blood cells, M/μL), HB (hemoglobin, g/dL), HCT (Hematocrit, %), MCV (mean corpuscular volume, fL), MCH (mean corpuscular hemoglobin, pg), MCHC (mean corpuscular hemoglobin concentration, g/dL), RDW (RBC distribution width, %), (C) PLT (platelet count, K/μL), MPV (mean platelet volume, fL). (D) Percent of CD8+, CD4+, and CD19+ cells (% in lymphocytes).

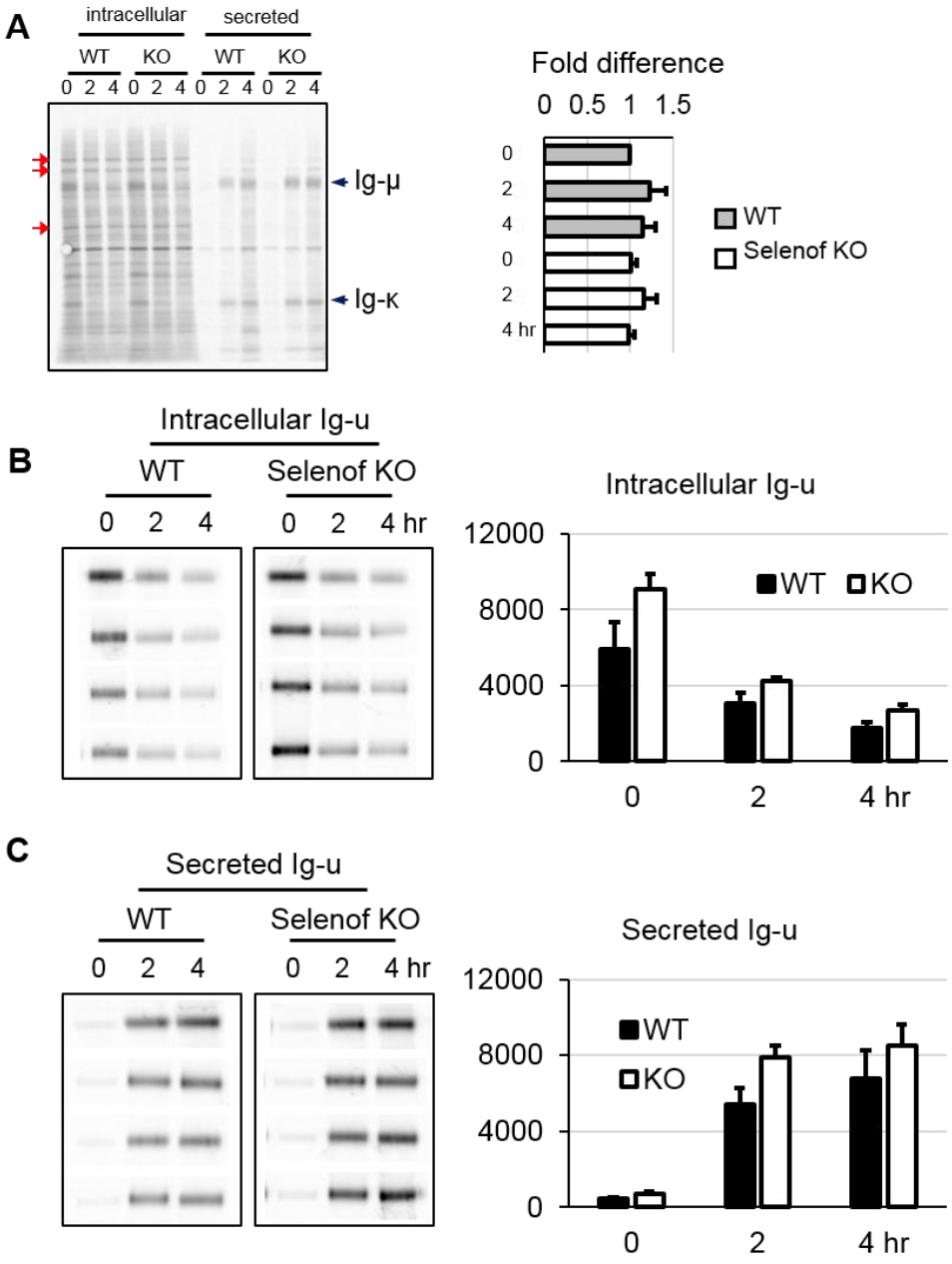

Figure S3. Kinetics of IgM biosynthesis and transport by radioactive pulse-chase assay, related to Fig. 2. (A) Intracellular and secreted proteins resolved in SDS-PAGE at differentiating day 3 plasma B cells isolated from WT and Selenof KO mice. Same number of cells were used for the analyses and additional protein quantification was accessed with levels of non-specific bands (marked with red arrows). (B) Intracellular Ig-μ and (C) secreted Ig-μ were measured under reducing conditions from biological and technical replicate samples. The Ig-μ expression levels were measured and compared using ImageJ. The artificial units were used in x-axis.

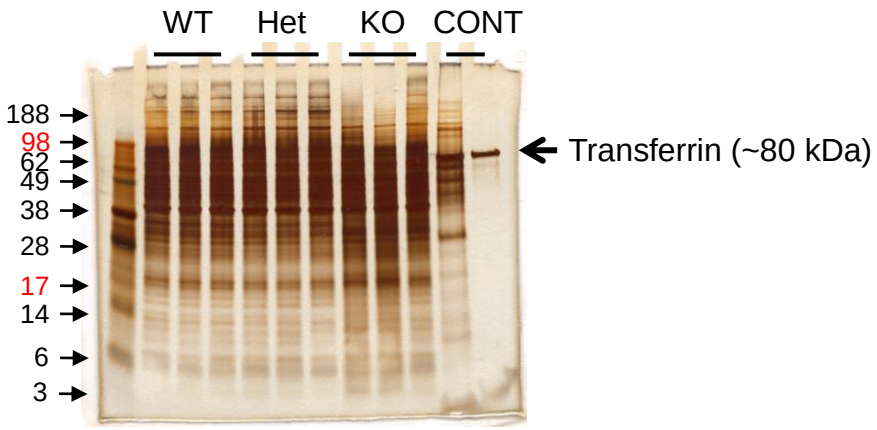

Figure S4. Silver stained proteins from cell pellets of Selenof MEFs, related to Fig. 6. WT, heterozygous (Het), and Selenof KO MEFs were cultured under serum starvation conditions. Lane 1; protein markers, lanes 2-4; WT MEFs, lanes 5-7; Het MEFs, lanes 8-10; KO MEFs, lane 11; concentrated cell culture medium obtained from WT MEFs, and lane 12; concentrated fresh culture medium (equal volume with lane 11) which was supplemented with insulin, transferrin, and selenium.

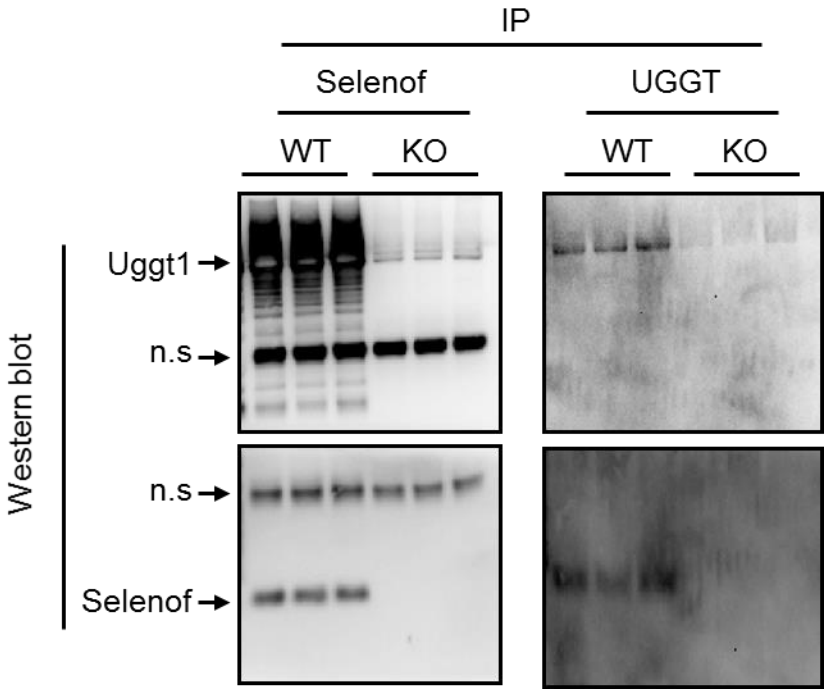

Figure S5. Selenof interaction with UGGT1, related to Fig. 6. Cell lysates from livers of WT and KO mice (3 animals per group) were subjected for immunoprecipitation with anti-Selenof or anti-UGGT1 antibodies. The IP products were characterized by Western blot analysis using anti-Selenof or anti-UGGT1 antibodies. Bands at ~15 kDa (Selenof) and ~170 kDa (UGGT1) were observed (indicated by arrows). Non-specific bands (n.s.) correspond to the antibody light chain (~25 kDa) and heavy chain (~ 50 kDa).

Supplemental Tables

Table S1, related to Table 1. Pathway enrichment analysis of proteins downregulated in Selenof KO MEFs.

Pathway name	Proteins found	Proteins Total	Ratio	p-value	FDR
Antigen Presentation: Folding, assembly and peptide loading of class I MHC	11	118	0.011	9.89E-07	0.000591
Antigen processing-Cross presentation	12	176	0.016	7.65E-06	0.0018
Endosomal/Vacuolar pathway	9	97	0.009	1.02E-05	0.0018
ER-Phagosome pathway	11	154	0.014	1.21E-05	0.0018
Interferon alpha/beta signaling	8	138	0.013	7.55E-04	0.0789
Interferon gamma signaling	9	174	0.016	7.96E-04	0.0789
Class I MHC mediated antigen processing & presentation	13	368	0.033	2.00E-03	0.169
WNT5A-dependent internalization of FZD2, FZD5 and ROR2	2	5	0	2.29E-03	0.169
PCP/CE pathway	6	98	0.009	2.64E-03	0.174
Signaling by NOTCH1 t(7;9)(NOTCH1:M1580_K2555) Translocation Mutant	2	8	0.001	5.71E-03	0.308
Constitutive Signaling by NOTCH1 t(7;9)(NOTCH1:M1580_K2555) Translocation Mutant	2	8	0.001	5.71E-03	0.308
Sema4D induced cell migration and growth-cone collapse	3	28	0.003	7.25E-03	0.33
Interferon Signaling	10	289	0.026	7.47E-03	0.33
Beta-catenin independent WNT signaling	7	162	0.015	7.87E-03	0.33
Laminin interactions	3	31	0.003	9.54E-03	0.372
Zinc influx into cells by the SLC39 gene family	2	11	0.001	1.05E-02	0.372
Non-integrin membrane-ECM interactions	4	61	0.006	1.08E-02	0.372
Sema4D in semaphorin signaling	3	33	0.003	1.13E-02	0.372
Semaphorin interactions	4	73	0.007	1.95E-02	0.427
Constitutive Signaling by NOTCH1 HD Domain Mutants	2	16	0.001	2.12E-02	0.427

Table S2, related to Table 1. Pathway enrichment analysis of proteins upregulated in Selenof KO MEFs.

Pathway name	Proteins found	Proteins Total	Ratio	p-value	FDR
COPII (Coat Protein 2) Mediated Vesicle Transport	6	75	0.007	1.29E-04	0.0233
ER to Golgi Anterograde Transport	8	157	0.014	2.18E-04	0.0233
MHC class II antigen presentation	7	141	0.013	6.34E-04	0.0545
Transport to the Golgi and subsequent modification	8	212	0.019	1.52E-03	0.108
Kinesins	4	50	0.005	1.79E-03	0.109
5-Phosphoribose 1-diphosphate biosynthesis	2	9	0.001	3.91E-03	0.19
Laminin interactions	3	31	0.003	4.05E-03	0.19
Cargo concentration in the ER	3	37	0.003	6.58E-03	0.257
Membrane Trafficking	9	340	0.031	8.09E-03	0.275
COPI Mediated Transport	2	14	0.001	9.16E-03	0.275
Golgi to ER Retrograde Transport	2	14	0.001	9.16E-03	0.275
Asparagine N-linked glycosylation	9	377	0.034	1.51E-02	0.38
Fatty Acyl-CoA Biosynthesis	4	95	0.009	1.65E-02	0.38
Recycling pathway of L1	3	53	0.005	1.72E-02	0.38
Regulation of PAK-2p34 activity by PS-GAP/RHG10	1	2	0	2.01E-02	0.38
XBP1(S) activates chaperone genes	4	102	0.009	2.08E-02	0.38
IRE1alpha activates chaperones	4	106	0.01	2.35E-02	0.38
ERK/MAPK targets	2	25	0.002	2.72E-02	0.38
Nuclear Events (kinase and transcription factor activation)	2	28	0.003	3.34E-02	0.427
Association of TriC/CCT with target proteins during biosynthesis	2	30	0.003	3.79E-02	0.427

Table S3, related to Table 1. Enriched functions identified by DAVID. Proteins whose expression differs between WT and Selenof KO MEFs under conditions of serum deprivation were analyzed for functional annotation clustering and the top three clusters are shown in the table.

Annotation Cluster 1	**Enrichment Score: 3.65**	**Count**	**p-value**	**Benjamini**
GOTERM_BP_FAT	Golgi vesicle transport	10	4.20E-05	6.70E-02
GOTERM_CC_FAT	cytoplasmic membrane-bounded vesicle	20	1.10E-04	1.00E-02
GOTERM_CC_FAT	membrane-bounded vesicle	20	1.70E-04	9.40E-03
GOTERM_CC_FAT	cytoplasmic vesicle	21	2.90E-04	1.00E-02
GOTERM_CC_FAT	vesicle	21	5.00E-04	1.40E-02
GOTERM_BP_FAT	vesicle-mediated transport	18	1.00E-03	4.30E-01
Annotation Cluster 2	**Enrichment Score: 2.84**	**Count**	**p-value**	**Benjamini**
GOTERM_BP_FAT	Golgi vesicle transport	10	4.20E-05	6.70E-02
GOTERM_CC_FAT	Golgi apparatus	26	1.80E-04	7.10E-03
GOTERM_BP_FAT	intracellular transport	20	6.50E-04	4.10E-01
GOTERM_BP_FAT	vesicle-mediated transport	18	1.00E-03	4.30E-01
SP_PIR_KEYWORDS	protein transport	15	1.10E-03	3.50E-02
GOTERM_BP_FAT	protein transport	21	1.50E-03	4.00E-01
GOTERM_BP_FAT	establishment of protein localization	21	1.70E-03	3.80E-01
GOTERM_BP_FAT	protein localization	22	3.80E-03	5.00E-01
SP_PIR_KEYWORDS	transport	31	5.70E-03	1.20E-01
GOTERM_BP_FAT	cellular protein localization	13	6.00E-03	5.40E-01
GOTERM_BP_FAT	cellular macromolecule localization	13	6.40E-03	5.30E-01
GOTERM_BP_FAT	intracellular protein transport	12	8.00E-03	5.60E-01
Annotation Cluster 3	**Enrichment Score: 2.02**	**Count**	**p-value**	**Benjamini**
GOTERM_BP_FAT	protein complex assembly	15	4.90E-03	5.20E-01
GOTERM_BP_FAT	protein complex biogenesis	15	4.90E-03	5.20E-01
GOTERM_BP_FAT	protein homooligomerization	6	7.10E-03	5.40E-01
GOTERM_BP_FAT	macromolecular complex subunit organization	18	8.50E-03	5.60E-01
GOTERM_BP_FAT	macromolecular complex assembly	16	2.10E-02	7.70E-01
GOTERM_BP_FAT	protein oligomerization	7	2.30E-02	7.60E-01

Supplemental Experimental Procedures

Western blotting. Total MEF and tissue proteins were prepared using protein lysis buffer containing protease inhibitor cocktails. For immunoblots, lysates were separated on NuPage Novex (10%) or Native PAGE (4-16%) Bis-Tris Gel system, typically 30 μg protein per lane, and transferred onto PVDF membranes. Membranes were incubated with 5% non-fat milk prior to incubation with primary antibodies for 4°C overnight. Blots were visualized using ECL Western Blotting Substrate and BioRad-ChemiDoc XRS+ molecular imager.

Microarray and Ingenuity Pathway Analyses. mRNA was isolated from spleens using Trizol, and microarray analyses were performed on Affymetrix Mouse 430_2.0A gene chips containing 45,000 gene probes. Three individual arrays were analyzed per genotype, and grouped results were compared by ANOVA using mAdb (NCI, NIH, Bethesda, MD). Those genes significantly different from the WT mice ($p<0.05$) were subjected to Ingenuity Pathway Analysis (Redwood City, CA), which significantly linked genes according to functional biological processes.

Plasma B cell immunoglobulin production assay. Secreted IgM levels during plasma B cell activation were measured daily using ELISA. Each day, a portion of differentiating plasma B cells were washed with PBS and OptiMem Medium by centrifugation. The cell pellets were resuspended in OptiMem medium and counted at a cell density of $1x10^6$ cells/ml. Differentiating B cells were then cultured in OptiMem medium to secret immunoglobulin. After 4 h, the cells and culture media were centrifuged twice at 300 g for 5 min, the spun media were saved and supplemented with protease inhibitors and 10 mM NEM. The secreted IgM levels were accessed from cell-free, centrifuged media using ELISA.

Enzyme-linked immunosorbent assay. Analysis of antigen-specific immunoglobulin titers in serum and B cell culture media was performed with capture ELISA. ELISA plates were prepared by pre-coating with capture antibodies, either rabbit anti-mouse Ig μ-chain or goat anti-mouse Ig (H+L) antibodies. To access the secreted immunoglobulin levels during plasma B cell differentiation, aliquots of diluted (1:10) media obtained from plasma B cell immunoglobulin secretion assay were added to anti-Ig μ-chain coated plates and incubated overnight at 4°C. After extensive washes, anti-μ-HRP (1:1,000) was added and incubated for 1 h at room temperature. The assay was developed with Sigma OPD fast read and the plates were read at 450 nm.

The WT and Selenof KO sera were used to determine immunoglobulin levels. Sera were diluted at 1:12,000 or 1:50,000 to determine immunoglobulin levels using anti-mouse Ig μ-chain coated plates or anti-Ig(H+L) coated plates, respectively. Detecting antibodies were either goat anti-mouse Ig κ-chain HRP or a series of immunoglobulin antibodies, and the plates were read at 450 nm using a plate reader.

Flow cytometry. For the staining of cell surface molecules, splenocytes or cultured cells from *in vitro* experiments were stained in FACS buffer (PBS, 1% FBS, 2 mM EDTA) with saturating concentrations of antibodies against indicated antigens at 4 °C. For intracellular staining, cells were fixed and permeabilized using the Foxp3 fix/perm kit (eBioscience) according to the manufacturer's instructions. Fc gamma receptor blocking antibody (anti-CD16/CD32) was added to prevent non-specific binding and dead cells were excluded from the analysis by using LIVE/DEAD fixable dead cell stain (Thermo Fisher). Flow cytometry was performed on an LSR II instrument (BD Biosciences) and data were analyzed using FlowJo v10.1 (FlowJo, LLC). In some experiments, B cells were purified, *in vitro* stimulated with LPS as described above, and the distribution of surface and intracellular IgM was analyzed at the indicated time points.

Neutrophil isolation for bacteria killing assay. Murine bone-marrow derived neutrophils were isolated from 12-week old C57BL/6J WT male animals. Hind limbs were aseptically harvested, the distal tips of each extremity were severed and bone marrow cells were flushed from femurs and tibias. Neutrophils from mouse bone marrow cells were isolated using negative depletion of other cell populations with a Neutrophil Isolation Kit (Miltenyi Biotec). The purity of neutrophils, as determined by Wright-Giemsa-staining method, was consistently greater than 98%.

***In vitro* bacteria killing assay.** Blood was withdrawn from the submandibular vein of WT and Selenof KO male mice, and the sera were separated using BD Microtainer serum separator tubes. Fresh overnight cultures of *S. aureus* (ATCC strain 10390) and *E. coli* (ATCC strain 19138) grown in Luria-Bertani medium were diluted 10-fold with fresh LB culture media and incubated for an additional 2 h at 37 ºC. Bacteria were pelleted by centrifugation, washed twice with PBS, and resuspended in PBS at an OD = 0.2 at 600 nm. Bacteria were opsonized with 10% (v/v) WT or Selenof KO mouse serum for 1 h at 37 ºC on an end-to-end rotator. The opsonized bacteria and neutrophils obtained from WT animals were mixed together at a 1:5 ratio for *E. coli* and 1:10 ratio for *S. aureus* (calculated by cell numbers) and incubated for 0, 30, 60 and 120 min at 37 ºC with intermittent shaking. After each incubation period, cells were lysed by adding double-distilled water, and the diluted aliquots were spread on LB agar (*E. coli*) or blood agar (*S. aureus*) plates. Colonies were counted after incubating the plates overnight at 37 ºC. Bacterial suspensions without any neutrophils added served as controls for each time point.

***In vivo* bacteria killing assay.** Freshly grown *E. coli* cells were harvested and washed twice with sterile PBS. Eight-twelve week old WT and Selenof KO male mice were challenged by intraperitoneal

injection of *E. coli* with 10^7 cfu in 500 µl of sterile PBS. Four hours after *E. coli* administration, the animals were euthanized and peritoneal lavage fluid was washed with 10 ml of sterile PBS. The lavage fluid was serially diluted with double-distilled water, then aliquots of serial dilutions were incubated on LB agar plates overnight at 37 °C. The number of colony forming bacteria was counted and the survival rate of *E. coli* determined.

Radioactive pulse and chase assay. Kinetics of IgM biosynthesis and transport were measured with a radioactive pulse-chase assay (Anelli et al., 2002; Cals et al., 1996; Mezghrani et al., 2001). Intracellular and secreted IgM were measured in primary B cells isolated from WT and Selenof KO mice. At day three of B cell differentiation, cells were incubated for 30 min in DMEM without methionine and cysteine supplemented with 1% dialyzed FCS, pulsed for 15 min with ^{35}S-labeled amino acids (220 µCi/10^6 cells) (Easy Tag, Perkin Elmer), washed and chased in complete medium for the indicated time-points. At time 0, 2, 4 h, the cells were treated with 10 mM NEM to prevent disulfide interchange and lysed in RIPA. Subsequently, lysates were immunoprecipitated with rabbit anti-mouse IgM antibodies (ThermoFisher Scientific #616800), cross-linked to protein G agarose beads. The beads were washed in 0.5 M NaCl, 0.5% SDS, 10 mM Tris-HCl pH 7.5, eluted in Laemmli buffer. Aliquots of the total cell lysates and immunoprecipitates were resolved by SDS-PAGE under non-reducing or reducing conditions and transferred to nitrocellulose. Membranes were then visualized by autoradiography with FLA900 Starion (FujiFilm Life Science, Tokyo, Japan). Densitometric quantification of the signals was performed with ImageJ.

Supplemental References

Anelli, T., Alessio, M., Mezghrani, A., Simmen, T., Talamo, F., Bachi, A., and Sitia, R. (2002). ERp44, a novel endoplasmic reticulum folding assistant of the thioredoxin family. EMBO J. *21*, 835-844.

Cals, M. M., Guenzi, S., Carelli, S., Simmen, T., Sparvoli, A., and Sitia, R. (1996). IgM polymerization inhibits the Golgi-mediated processing of the mu-chain carboxy-terminal glycans. Mol. Immunol. *33*, 15-24.

Mezghrani, A., Fassio, A., Benham, A., Simmen, T., Braakman, I., and Sitia, R. (2001). Manipulation of oxidative protein folding and PDI redox state in mammalian cells. EMBO J. *20*, 6288-6296.